Neurobiology of Disease

Risperidone Ameliorates Prefrontal Cortex Neural Atrophy and Oxidative/Nitrosative Stress in Brain and Peripheral Blood of Rats with Neonatal Ventral Hippocampus Lesion

Hiram Tendilla-Beltrán,[1,2,3,4] Silvia Meneses-Prado,[1] Rubén Antonio Vázquez-Roque,[1] Miguel Tapia-Rodríguez,[5] Andrea Judith Vázquez-Hernández,[1] Heriberto Coatl-Cuaya,[1,2] David Martín-Hernández,[3,4,6,7] Karina S. MacDowell,[3,4,6,7] Linda Garcés-Ramírez,[2] Juan C. Leza,[3,4,6,7] and Gonzalo Flores[1]

[1]Instituto de Fisiología, Benemérita Universidad Autónoma de Puebla (BUAP), Puebla, 72570, Mexico, [2]Departamento de Fisiología, Escuela Nacional de Ciencias Biológicas, Instituto Politécnico Nacional, CDMX, 11340, Mexico, [3]Departamento de Farmacología y Toxicología, Facultad de Medicina, and [4]Instituto Universitario de Investigación en Neuroquímica, Universidad Complutense de Madrid, Madrid, 28040, Spain, [5]Instituto de Investigaciones Biomédicas, Universidad Nacional Autónoma de México, CDMX, 04510, Mexico, [6]Centro de Investigación Biomédica en Red de Salud Mental, Madrid, 28029, Spain, and [7]Instituto de Investigación Sanitaria Hospital 12 de Octubre, Madrid, 28041, Spain

Reduction of the dendritic arbor length and the lack of dendritic spines in the pyramidal cells of the prefrontal cortex (PFC) are prevalent pathological features in schizophrenia (SZ). Neonatal ventral hippocampus lesion (NVHL) in male rats reproduces these neuronal characteristics and here we describe how this is a consequence of BDNF/TrkB pathway disruption. Moreover, COX-2 proinflammatory state, as well as Nrf-2 antioxidant impairment, triggers oxidative/nitrosative stress, which also contributes to dendritic spine impairments in the PFC. Interestingly, oxidative/nitrosative stress was also detected in the periphery of NVHL animals. Furthermore, risperidone treatment had a neurotrophic effect on the PFC and antioxidant effects on the brain and periphery of NVHL animals; these cellular effects were related to behavioral improvement. Our data highlight the link between brain development and immune response, as well as several other factors to understand mechanisms related to the pathophysiology of SZ.

Key words: **BDNF/TrkB pathway; COX-2; neonatal ventral hippocampus lesion; oxidative/nitrosative stress; prefrontal cortex; risperidone**

Significance Statement

Prefrontal cortex dysfunction in schizophrenia can be a consequence of morphological abnormalities and oxidative/nitrosative stress, among others. Here, we detailed how impaired plasticity-related pathways and oxidative/nitrosative stress are part of the dendritic spine pathology and their modulation by atypical antipsychotic risperidone treatment in rats with neonatal ventral hippocampus lesion. Moreover, we found that animals with neonatal ventral hippocampus lesion had oxidative/nitrosative stress in the brain as well as in the peripheral blood, an important issue for the translational approaches of this model. Then, risperidone restored plasticity and reduced oxidative/nitrosative stress of prefrontal cortex pyramidal cells, and ultimately improved the behavior of lesioned animals. Moreover, risperidone had differential effects than the brain on peripheral blood oxidative/nitrosative stress.

Introduction

In 1972 Frederick Plum referred to schizophrenia (SZ) as "the graveyard of the neuropathologists", because of the lack of determinant pathophysiological data (Plum, 1972). More than 4 decades later, the etiology and mechanisms of the disease are still unclear, despite the many approaches that have been made to

Received May 29, 2019; revised Aug. 7, 2019; accepted Aug. 31, 2019.

Author contributions: H.T.-B., R.A.V.-R., D.M.-H., L.G.-R., J.C.L., and G.F. designed research; H.T.-B., S.M.-P., R.A.V.-R., A.J.V.-H., H.C.-C., D.M.-H., and K.S.M. performed research; J.C.L. and G.F. contributed unpublished reagents/analytic tools; H.T.-B., S.M.-P., M.T.-R., K.S.M., L.G.-R., and G.F. analyzed data; H.T.-B., J.C.L., and G.F. wrote the paper.

This work was supported by the Spanish Ministry of Economy, Industry and Competitiveness (MINECO-EU-FEDER) SAF2016-75500-R to J.C.L. and PRODEP (CA-BUAP-120) and the CONACYT Grant (252808) to G.F.; H.T.-B. and H.C.-C. acknowledge CONACYT for scholarship; and R.A.V.-R., M.T.-R., L.G.-R., and G.F. acknowledge the "Sistema Nacional de Investigadores" of Mexico for memberships. None of the funding institutions had any further role in the study design, the collection of data, analyses, and interpretation of data, writing of the report, or in the decision to submit the paper for publication. We thank Francisco Ramos Collazo for help with the animal care, Sandra Rodríguez-Maus for help with the biochemical experiments, and Robert Simpson for editing the English language text.

The authors declare no competing financial interests.

Correspondence should be addressed to Juan C. Leza at jcleza@med.ucm.es or Gonzalo Flores at gonzaloflores56@gmail.com.

https://doi.org/10.1523/JNEUROSCI.1249-19.2019

clarify it. Interestingly, the reduction of the dendritic arbor length and the lack of dendritic spines in the pyramidal cells of the prefrontal cortex (PFC) are prevalent pathological features (Garey et al., 1998; Glantz and Lewis, 2000; Konopaske et al., 2018). Many studies in SZ focus on the PFC because of its relation to cognitive functions that allow the individuals an adequate perception of the reality and a proper behavioral response. Because dendrites and dendritic spines are the main sites for excitatory synapses in the brain (Harris and Kater, 1994), their reduction alters PFC function in SZ, triggering various characteristic symptoms: psychosis, hallucinations, and anhedonia (Glausier and Lewis, 2013). It has been proposed that excessive synaptic pruning is the cause of the dendrites and spines lost in SZ and recent studies show that this could be a microglia-mediated phenomenon, due to complement activity or phagocytosis (Sekar et al., 2016; Sellgren et al., 2019). The aforementioned highlights the immune system as a potential link between early life insults in brain development and their late consequences, which finally onsets the disease (neurodevelopmental hypothesis of SZ; Weinberger, 1987; Potkin et al., 2009).

High levels of proinflammatory cytokines and immune markers, as well as an unbalanced inflammatory response in the peripheral blood of patients, have been detected (García-Bueno et al., 2014a,b; Leza et al., 2015; Dickerson et al., 2016). Also, postmortem studies have shown oxidative/nitrosative stress in the PFC (Andreazza et al., 2010, 2013; García-Bueno et al., 2016). Thus inflammation and oxidative/nitrosative stress also are implicated in the pathophysiology of SZ.

The neonatal ventral hippocampus lesion (NVHL) in the rat is an useful animal model to study some mechanisms involved in the pathophysiology of SZ (Tseng et al., 2009). Adult NVHL animals have dendritic arbor and spine pathology (Flores et al., 2005; Ryan et al., 2013; Tendilla-Beltrán et al., 2019), as well as oxidative/nitrosative stress in the PFC (Cabungcal et al., 2014). These cellular impairments result in various behavioral SZ-related abnormalities such as hyperlocomotion after exposure to dopaminergic agonists or a novel environment (Lipska et al., 1993; Flores et al., 1996; Alquicer et al., 2004), altered sensory gating (Le Pen et al., 2003; McDannald et al., 2011; Vázquez-Roque et al., 2012), and social isolation (Le Pen et al., 2000; Alquicer et al., 2008; Vázquez-Roque et al., 2012). Additionally, some of these brain and behavioral alterations can be reversed by antipsychotics (Sams-Dodd et al., 1997; Rueter et al., 2004; Bringas et al., 2012; Castellano et al., 2013).

Risperidone (RISP) is an atypical antipsychotic widely used in SZ therapy. In addition to its canonical antipsychotic pharmacological mechanism (dopamine D2 and serotonin 5-HT2A receptor antagonism; Kuroki et al., 2008), there is evidence that RISP modulates the inflammatory response. *In vitro* protocols have demonstrated that RISP treatment increases the levels of anti-inflammatory cytokines and reduces proinflammatory cytokines (Al-Amin et al., 2013; Brinholi et al., 2016). This effect has also been reported in patients, and also this substance decreases oxidative/nitrosative stress (Noto et al., 2014; Juncal-Ruiz et al., 2018). Even in an animal model of neuroinflammation, RISP was capable of reducing both inflammatory mediators and oxidative/nitrosative stress in the PFC (MacDowell et al., 2013).

In this study, we aim to determine the effects of RISP treatment on rats subjected to the SZ-like experimental model: the NVHL. For this purpose, we evaluated neuronal morphology and dendritic spine dynamics in the PFC. Furthermore, we studied inflammatory parameters and oxidative/nitrosative stress in the brain and peripheral blood. Finally, we also explored possible behavioral effects of RISP in rats with NVHL.

Materials and Methods

Animals

Pregnant Sprague-Dawley dams ($n = 10$) with 14–16 gestational days were obtained from our facilities (Autonomous University of Puebla and Harlan). Animals were individually housed in a temperature/humidity controlled environment in a 12 h light/dark cycle with *ad libitum* access to food and water. After birth, considered postnatal day (P)0, at P7 only male pups ($n = 68$) were randomly assigned for either sham ($n = 34$) or NVHL surgery ($n = 34$). On P21, animals were weaned and a similar number of sham and lesioned rats were placed in each cage (four animals per cage). At P89, the locomotor behavior of a group of animals ($n = 24$ sham and 24 NVHL) was evaluated. After this, all animals were administered with vehicle or RISP for 21 consecutive days. After treatment, the animals that were previously behaviorally tested were evaluated again for motor activity and social behavior. The morphological assessments were explored in these animals. Another group of animals (sham: $n = 10$, NVHL: $n = 10$) was killed immediately after treatment for the biochemical experiments (Fig. 1*A*). All procedures described in the present study were performed in accordance with the BUAP Animal Care Committee (FLAG-UALVIEP-17-1) and the *Guide for Care and Use of Laboratory Animals* of the Mexican Council for Animal Care (Norma Oficial Mexicana NOM-062-ZOO-1999), as well as the Animal Welfare Committee of Universidad Complutense in accordance with European legislation (2010/63/EU). All efforts were made to reduce the number of animals used and minimize animal suffering in the experiments.

Surgical procedures

NVHL protocol has been precisely described before (Lipska et al., 1993; Flores et al., 1996). On P7, male pups (weighing 15–18 g) were anesthetized using hypothermia. Then pups were positioned on a modified platform (Sierra et al., 2009) fixed to a stereotaxic Kopf Instrument, and subsequently 0.3 μl of ibotenic acid (10 μg/μl; Sigma-Aldrich) or an equal volume of vehicle (0.1 M PBS, pH 7.4) was bilaterally injected into the ventral hippocampus over a 2 min period through a 30-G stainless-steel cannula connected to an infusion pump through a Hamilton syringe positioned at the following coordinates: AP −3.0 mm, ML ±3.5 mm to bregma, and DV −5.0 mm from dura, according to the Paxinos and Watson (1986) rat brain atlas. After the procedure, pups were placed on a heating pad for recovery and returned to their dams.

Risperidone administration

At P90, sham and NVHL rats were administered (i.p.) either 0.25 mg/kg RISP (Janssen Pharmaceutica) dissolved in 0.25% glacial acetic acid and 0.1 M PBS or vehicle for 21 consecutive days. Four groups of animals were formed ($n = 17$/group): (1) sham-vehicle, (2) NVHL-vehicle, (3) sham-RISP, and (4) NVHL-RISP.

Behavioral tests

Behavioral observations were performed between 8:00–12:00 h in a noise-free, odorless room in which animals were acclimatized 24 h before tests.

Locomotor activity. The test was performed twice: before treatment (P89, $n = 24$ sham and 24 NVHL) and after RISP or vehicle administration (P111, $n = 12$/group). Locomotor activity was monitored for 120 min in 16 individual cages (20 × 40 × 30 cm), each of which was equipped with eight photobeam detectors connected to a computer counter (Tecnología Digital México). Each photobeam interruption by the rat was counted as locomotor activity (Morales-Medina et al., 2008).

Social interaction. One day after the post-treatment locomotor activity test, the social behavior of the animals was evaluated. The protocol was modified from the original method (File, 1980) and from a previous report from our group (Vázquez-Roque et al., 2012). Six pairs of rats from the same group (Sham-vehicle/Sham-vehicle, NVHL-vehicle/NVHL-vehicle, Sham-RISP/Sham-RISP, NVHL-RISP/NVHL-RISP) and that had no previous contact before were randomly organized and placed

into an open-field arena (60 × 60 × 60 cm) with dark walls. Their activity was recorded for 10 min, and videos were analyzed by a trained observer who was blind to the experiment obtaining the total number of interactions and the time spent during the active social behaviors. Only sniffing, following, grooming, mounting, wrestling, and jumping on or crawling under or over the partner behaviors were considered social behaviors.

Tissue samples

After the behavioral tests, the animals were deeply anesthetized (sodium pentobarbital 75 mg/kg, i.p.) and killed according to the needs of the respective protocols. One group of rats were used for the Golgi–Cox method (n = 8/group), these animals were perfused intracardially with physiological saline solution and their brains were extracted and preserved in Golgi–Cox solution. Another group of rats was subjected to the stereology protocol (n = 4/group), these animals were perfused intracardially with physiological saline solution followed by 4% paraformaldehyde in 0.1 M PBS and brains were extracted and preserved in 4% paraformaldehyde. Another group of animals (n = 5/group) was used for biochemical assays. After anesthesia, intracardial blood samples were obtained and located in EDTA, then the brain was removed from the skull and the PFC was excised and frozen at −80°C until assayed.

Neuronal morphology

Golgi–Cox stain method

To evaluate the effects of RISP on neural morphology in the PFC neurons of NVHL rats, a modified Golgi–Cox stain method was used (Gibb and Kolb, 1998). Coronal brain sections of 200 μm thickness at the level of PFC were obtained using a vibratome (Campden Instruments, MA752) and placed on clean gelatin-coated microscope slides for the revealing process: slides were treated with ammonium hydroxide (30 min in dark), then with Kodak Film Fixer (30 min in dark) and afterward washed with distilled water, dehydrated, and whitened in successive baths of 50% (1 min), 75% (1 min), 90% (1 min), and 100% (2 × 5 min) ethanol, followed by 15 min in xylene. Finally, slides were mounted with a synthetic resin medium.

Microscopic observation, Sholl analysis, dendritic spine density, and classification

Bi-dimensional reconstruction of the entire basilar dendritic arbor of pyramidal PFC neurons located in layers 3 and 5 (area Cg1; plate 7–9) according to the Paxinos and Watson (1986) rat brain atlas, was reproduced for each neuron. For each animal, five neurons from each hemisphere were drawn using a camera Lucida at 400× magnification (DMLS 2000, Leica Microscope). Dendritic tracings were quantified using Sholl analysis placing a transparent grid with equidistant (10 μm) concentric rings centered over the tracings, and the number or ring-dendrite intersections was used to estimate the total dendritic length and

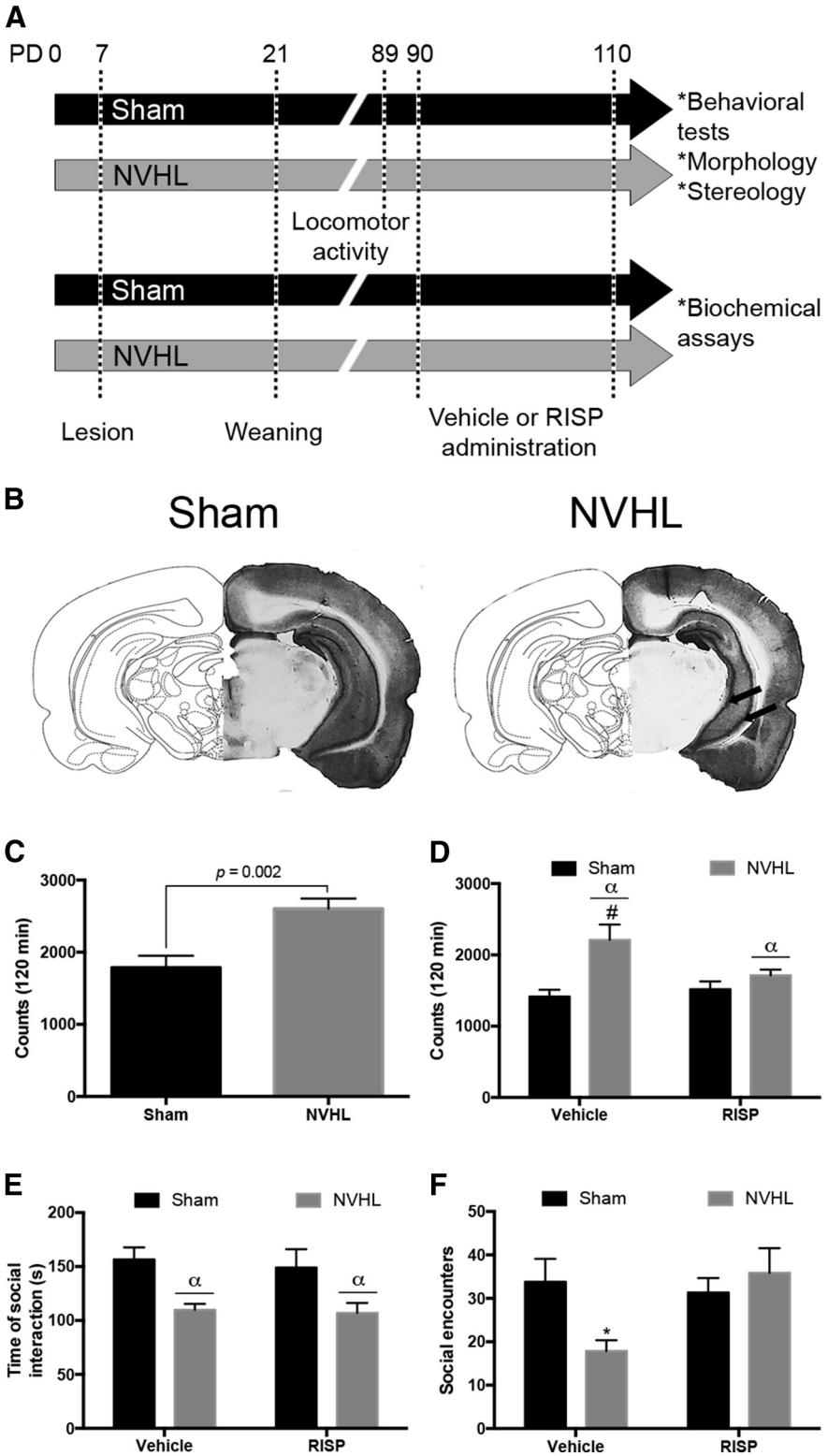

Figure 1. ***A***, Diagram illustrating the experimental protocol (PD: postnatal day). ***B***, Representative coronal photographs of the sham lesion and NVHL, arrows indicate the site of the lesion. ***C***, ***D***, Locomotor behavior was evaluated before and after treatment. ***C***, before treatment (n = 24/group), NVHL animals exhibited hyperlocomotion (U = 144, p = 0.002). ***D***, After vehicle or RISP administration (n = 12/group), RISP reduced the number of movements in NVHL rats ($^{\alpha}$lesion effect: $p < 0.001$; $^{\#}p < 0.05$ vs NVHL-RISP, $p < 0.01$ vs sham-RISP, $p < 0.001$ vs sham-vehicle). ***E***, ***F***, Social behavior was evaluated only after treatment (n = 6/group). ***E***, NVHL rats spent less time in social behavior and RISP did not affect this parameter ($^{\alpha}$lesion effect: $p = 0.001$). ***F***, The NVHL reduced the number of social encounters and RISP enhanced the number of encounters ($^{*}p < 0.05$ vs all the other groups). Statistical analyses for locomotor behavior before treatment were conducted using a Mann–Whitney U test; for the rest of parameters a two-way ANOVA, Newman Keuls *post hoc* test was used.

Table 1. Optical fractionator sampling parameters used for neural counting

Parameter	Value
No. of sections, range	9–15
Distance between sections, μm	150
Scan grid, μm	800 × 800
Counting frame, μm	60 × 60
Disector height, μm	20
Guard zones (upper and lower), μm	10
Average section thickness, μm (range)	35.98 (33.2–38.1)

length per dendritic order (Sholl and Uttley, 1953). To calculate the spine density, a 30 μm approximated segment of distal dendrite was traced (at 1000×) and the number of spines was counted (to yield spines/10 μm). For dendritic spine dynamics, 100 hundred distal dendritic spines were manually classified (at 2000×) according to shape in six different categories: thin (elongated with similar head/neck diameter), mushroom (prominent head with defined neck), stubby (unrecognizable neck), bifurcated (with 2 heads), multi-headed (>2 heads), and unclassified (without complying with any the previous criteria; Brusco et al., 2010; Bello-Medina et al., 2016; Tendilla-Beltrán et al., 2019).

Neuronal density

Stereological analysis

Before sectioning, brains were placed in a sucrose gradient and then 50-μm-thick coronal sections from PFC were obtained using a cryostat (Leica, CM1510-1) and mounted on gelatin-coated microscope slides. For stereological analysis, brain slices were stained with cresyl violet and systematically random sampled with an optical fractionator probe (Vázquez-Roque et al., 2012, 2014; Romero-Pimentel et al., 2014). Neurons were identified by their size and shape (Chareyron et al., 2012), using a MBF CX9000 color CCD camera (MicroBrightField) coupled to an Olympus BX51WI microscope and sampled at 60× (UPlanSAPO 60× N.A. 1.20 water-immersion objective, Olympus) with the aid of StereoInvestigator v9.14.5 (MicroBrightField). Sampling parameters used for cell counting are shown in Table 1.

Biochemical assays

Plasma, peripheral blood mononuclear cells, and PFC sample collection

Immediately after obtained, blood samples were centrifuged at 1800 rpm for 10 min at 4°C and plasma was collected and frozen at −80°C. The residual sample was diluted (1:1) with RPMI media and loaded into Ficoll solution (0.65 ml of Ficoll by 1 ml of sample) and centrifuged at 2000 rpm for 40 min at room temperature. Then, the mononuclear cell phase was obtained and diluted again in 15 ml of RPMI and centrifuged at 3000 rpm for 15 min at room temperature. The supernatant was decanted and the obtained pellet was resuspended in 1 ml of RPMI and centrifuged at 3000 rpm for 10 min at room temperature. The supernatant was eliminated and the pellets, which represented the peripheral blood mononuclear cells (PBMCs), were frozen at −80°C until assayed.

Cytosolic and nuclear extraction

To obtain cytosolic fraction and nuclear extracts, a previously reported procedure was used (Martin-Hernandez et al., 2019). Shortly, PFC and PBMC samples were homogenized in 300 μl buffer (10 mmol/L *N*-2-hydroxyethylpiperazine*N*-2-ethanesulfonic acid, pH 7.9, 1 mmol/L EDTA, 1 mmol/L EGTA, 10 mmol/L KCl, 1 mmol/L dithiothreitol, 0.5 mmol/L phenylmethylsulfonyl fluoride, 0.1 mg/ml aprotinin, 1 mg/ml leupeptin, 1 mg/ml Na-p-tosyll-lysine-chloromethyl ketone, 5 mmol/L NaF, 1 mmol/L $NaVO_4$, 0.5 mol/L sucrose, and 10 mmol/L Na_2MoO_4). After 15 min, Nonidet P-40 (Roche) was added to reach a 0.5% concentration. The tubes were gently vortexed for 15 s and nuclei were collected by centrifugation at 8000 × *g* for 5 min. Supernatants were considered the cytosolic fraction. The pellets were resuspended in 100 μl buffer supplemented with 20% glycerol and 0.4 mol/L KCl and gently shaken for 30 min at 4°C. Nuclear protein extracts were obtained by centrifugation at 13,000 × *g* for 5 min and aliquots of the supernatant were stored at −80°C.

Western blot protocol

Briefly, after quantifying and adjusting protein levels, the PFC and PBMC homogenates were mixed with Laemmli buffer (Bio-Rad) and 20 μl (1 μg/μl) was loaded in acrylamide electrophoresis gel. Once the proteins were separated due their molecular weight, they were transferred to a nitrocellulose membrane (Transfer-Blot Turbo Transfer Pack, Bio-Rad) with a semidry transfer system (Bio-Rad). Then membranes were incubated with specifically diluted antibodies in TBS-Tween, sometimes added with bovine serum albumin (BSA): rabbit monoclonal anti-BDNF (1:1000; Abcam, ab108319; RRID:AB_10862052), rabbit polyclonal anti-TrkB (1:1000, 1% BSA; Santa Cruz Biotechnology, sc8316; RRID:AB_2155274), rabbit polyclonal anti-PI3K (1:750, 1% BSA; Santa Cruz Biotechnology, sc7189; RRID:AB_2165408), rabbit polyclonal anti-Ser437phospho-Akt (1:1000; Cell Signaling Technology, 4060; RRID:AB_2315049), rabbit polyclonal anti-Akt (1:1000; Cell Signaling Technology, 4691; RRID:AB_915783), rabbit polyclonal anti-Thr202/Tyr204phospho-ERK (1:1000; Cell Signaling Technology, 8544; RRID:AB_11127856), rabbit polyclonal anti-ERK (1:1000; Cell Signaling Technology,#4695; RRID:AB_390779), rabbit polyclonal anti-IκBα (1:1000; Santa Cruz Biotechnology, sc371; RRID:AB_2235952); rabbit polyclonal anti-NF-κB p65 (1:1000; Santa Cruz Biotechnology, sc372; RRID:AB_632037), goat polyclonal anti-COX-2 (1:750, 2.5% BSA; Santa Cruz Biotechnology, sc1747; RRID:AB_2084976), rabbit polyclonal anti-PPAR-γ (1:1000; Santa Cruz Biotechnology, sc7196; RRID:AB_654710), rabbit polyclonal anti-iNOS (1:750 1%BSA; Santa Cruz Biotechnology, sc650; RRID:AB_2298577), mouse monoclonal anti-4-hydroxynonenal (1:500, 3% BSA; R&D Systems, MAB3249; RRID:AB_664165), goat polyclonal anti-Ser9phospho-GSK-3β (1:750, 1% BSA; Santa Cruz Biotechnology, sc11757; RRID:AB_2279471); rabbit polyclonal anti-GSK-3β (1:1000; Santa Cruz Biotechnology, sc9166; RRID:AB_647604), mouse monoclonal anti-Keap1 (1:1000; R&D Systems, MAB3024; RRID:AB_2132620); rabbit polyclonal anti-Nrf2 (1:1000; Santa Cruz Biotechnology, sc722; RRID:AB_2108502). After washing with TBS-Tween solution, proteins were identified by incubating membranes with the respective horseradish peroxidase-conjugated secondary antibody (1:2000) for 90 min at room temperature and revealed by ECLTM-kit following the manufacturer's instructions (GE Healthcare).

Transfer blots were imaged using the Odyssey Fc System (Li-COR Biosciences) and densitometrically quantified (NIH ImageJ software). All densitometries are expressed in arbitrary units of optical density. Housekeeping proteins were β-actin (1:15000; Sigma-Adrich, A5441; RRID:AB_476744) for cytosolic extracts and GAPDH (1:5000; Sigma-Aldrich, G8795; RRID:AB_1078991) for nuclear ones.

Nitrites

PFC tissue were sonicated in 600 μl phosphate buffer (50 mmol/L). Nitrites (NO_2^-) were quantified in PFC homogenates and plasma using the Griess method (Green et al., 1982). In an acidic solution with 1% sulfanilamide and 0.1% *N*-(1-naftil) etilendiamide, NO_2^- turned into a pink compound photometrically measured in a microplate reader at 540 nm (Synergy 2, BioTek). NO_2^- concentration in samples was calculated using a $NaNO_2$ standard curve (1–25 μM).

Lipid peroxidation

The thiobarbituric acid method was used for lipid peroxidation determination (Das and Ratty, 1987). PFC and plasma samples were deproteinized with 40% trichloroacetic acid and HCl (5 mol/L), following the addition of 2% thiobarbituric acid (w/v) in NaOH (0.5 mol/L). The reaction was incubated in water bath at 90°C for 15 min and centrifuged at 12,000 rpm for 10 min. Pink chromogen was measured in a microplate reader at 532 nm (Synergy 2, BioTek). Malondialdehyde (MDA) concentration in samples was calculated using a MDA standard curve (0–100 nM).

Protein assay

Protein levels were measured using the Bradford method based on the protein-dye binding principle (Bradford, 1976).

Statistical analyses

The mean values of each animal were treated as a single measurement for data analysis. All data are presented as the mean ± SEM. Only data on the locomotor activity before treatment were analyzed using a Mann–Whitney *U* test. The rest of the data were analyzed using two-way ANOVA followed by the Newman–Keuls test for *post hoc* comparisons; for locomotor activity after treatment, social interaction, dendritic length, dendritic spine density, dendritic spine classification, neuronal density, and biochemical assays lesion and RISP treatment were considered as independent factors; and for length per dendritic order the independent factors were lesion and branch order. In all cases, $p < 0.05$ was considered the threshold for statistical significance. Also, *p* values were rounded off to 3 decimal places and when $p > 0.1$ it was just stated $p > 0.05$. Data were analyzed in GraphPad Prism 6.0.

Results

Verification of the lesion

Coronal sections at the level of the ventral hippocampus were obtained and stained with cresyl violet ($n = 68$). Then, sections were analyzed and loss of hippocampal integrity was observed in rats with NVHL; only rats with hippocampal damage were used for the present study ($n = 34$). Sham animals ($n = 34$) did not show any visible damage (Fig. 1*B*).

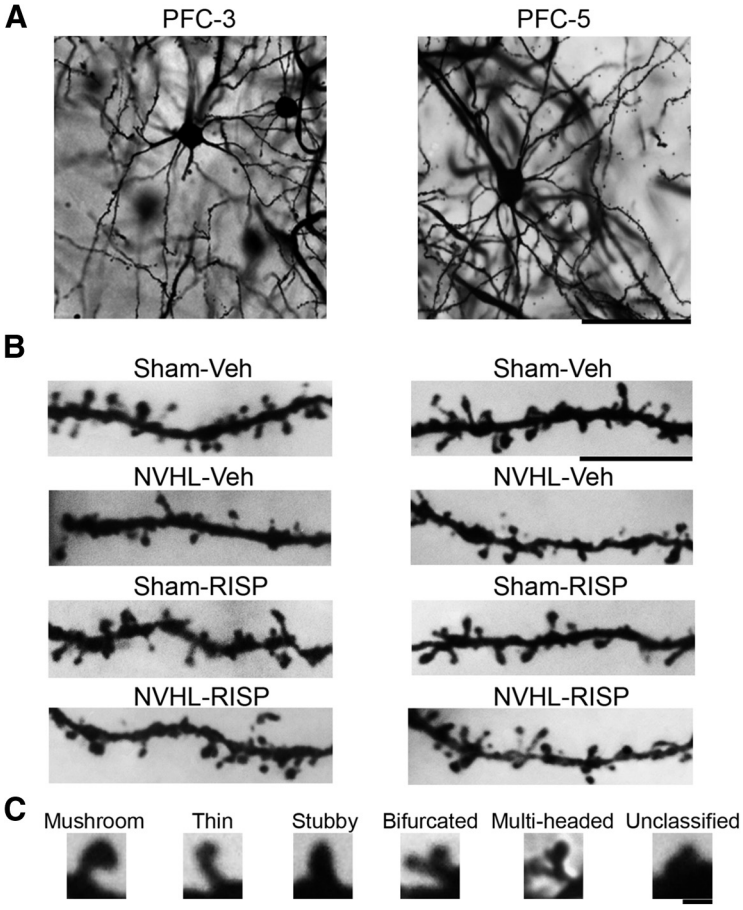

Figure 2. ***A***, Representative photomicrographs of the PFC layers 3 and 5 pyramidal neurons from the sham-vehicle group rat. Scale bar, 50 μm. ***B***, Dendritic segments of each group. Scale bar, 10 μm. ***C***, Examples of each type of dendritic spine according to its shape. Scale bar, 2 μm.

Behavioral results

Effects of RISP on the behavioral alterations of rats with NVHL

Locomotor activity was evaluated before and after pharmacological treatment. Before treatment, NVHL rats showed hyperactivity ($U = 144$, $p = 0.002$; Fig. 1*C*). After treatment, hyperactivity persisted in NVHL animals ($F_{(1,44)} = 13.51$, $p < 0.001$). Also, the interaction between the lesion and RISP was significant ($F_{(1,44)} = 4.989$, $p = 0.03$), and RISP reduced the number of movements of the NVHL animals (*post hoc*: $p < 0.05$). RISP treatment did not affect the locomotor behavior of sham animals ($F_{(1,44)} = 2.127$, $p > 0.05$; Fig. 1*D*).

In the social test, NVHL animals spent less time in social interaction, without a RISP effect (lesion: $F_{(1,20)} = 14.71$, $p = 0.001$; RISP: $F_{(1,20)} = 0.203$, $p > 0.05$; Fig. 1*E*). There was an interaction between the lesion and RISP factors in the number of social encounters ($F_{(1,20)} = 5.361$, $p = 0.031$), that was reduced only in the NVHL vehicle-treated group (*post hoc*: $p < 0.05$; Fig. 1*F*).

Morphological results

Effects of RISP on neuronal morphology and dendritic spine dynamics impairments in the PFC due to NVHL

The basal dendritic arbor length, dendritic spine density and dendritic spine morphological classification of 640 pyramidal neurons from PFC layers 3 and 5 was performed (Fig. 2). In the PFC layer 3 neurons, the NVHL reduced their total dendritic length ($F_{(1,28)} = 9.431$, $p = 0.004$) and RISP treatment increased it ($F_{(1,28)} = 5.869$, $p = 0.022$; Fig. 3*A*). The decrease in the dendritic arbor was because of the reduction of the second- and third-order dendrites' length only in the NVHL-vehicle group (interaction: $F_{(18,196)} = 2.396$, $p = 0.002$; lesion: $F_{(3,196)} = 7.079$, $p < 0.001$; dendritic order: $F_{(6,196)} = 526.2$, $p < 0.001$) and RISP treatment restored the length of both orders in NVHL animals (*post hoc*. second order: $p < 0.01$; third order: $p < 0.001$; Fig. 3*B*). Dendritic spine density decreased because of NVHL ($F_{(1,28)} = 4.667$, $p = 0.039$), increased as RISP effect ($F_{(1,28)} = 7.286$, $p = 0.011$), and there was an interaction between factors ($F_{(1,28)} = 9.911$, $p = 0.004$); the decrease in dendritic spine number as a consequence of NVHL got restored after RISP administration according with *post hoc* analyses ($p < 0.01$; Fig. 3*C*). Regarding the morphological classification of dendritic spines, the mushroom spine population decreased because of NVHL ($F_{(1,28)} = 20.99$, $p < 0.001$) and increased as a consequence of RISP treatment ($F_{(1,28)} = 10.06$, $p = 0.004$; Fig. 3*D*). Also, RISP increased the thin spine population ($F_{(1,28)} = 26.38$, $p < 0.001$), and the NVHL effect of reducing these kinds of spines was almost significant ($F_{(1,28)} = 4.192$, $p = 0.052$; Fig. 3*D*). In the stubby spine population, not only significant interaction between the lesion and RISP factors was found, but also the number of stubby spines increased as because of NVHL and decreased because of RISP (interaction: $F_{(1,28)} = 7.049$, $p = 0.013$; lesion: $F_{(1,28)} = 40.03$, $p < 0.001$; RISP: $F_{(1,28)} = 12.20$, $p = 0.002$); *post hoc* analyses revealed that RISP rescued this spine population in the NVHL animals ($p < 0.001$; Fig. 3*D*). Moreover, RISP decreased the number of bifurcated spines ($F_{(1,28)} = 33.88$, $p < 0.001$), without NVHL effect ($F_{(1,28)} = 1.962$, $p > 0.05$; Fig. 3*D*). The NVHL increased the number of multi-headed spines and RISP reduced them, also an interaction between the lesion and RISP was found (interaction: $F_{(1,28)} =$

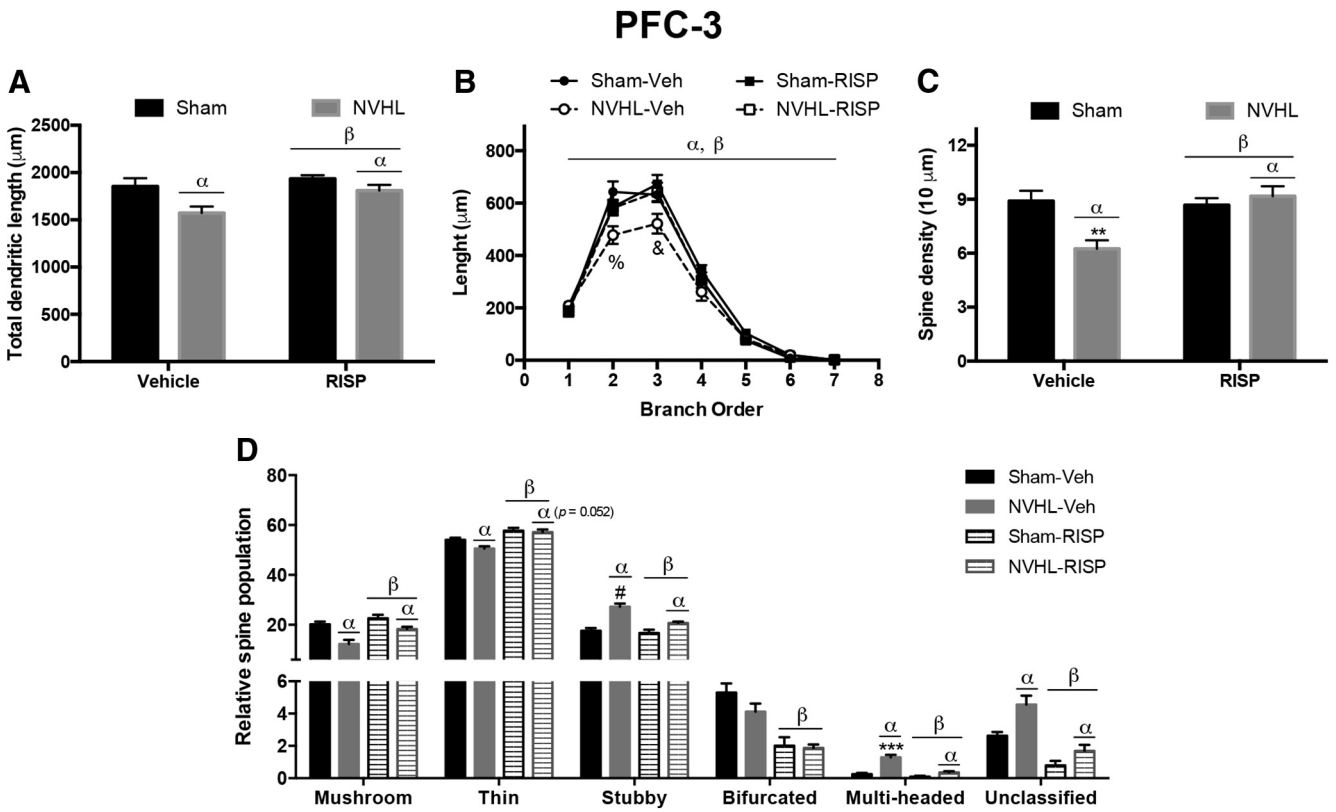

Figure 3. NVHL generates neural atrophy in the PFC layer 3 neurons that RISP treatment ameliorated ($n = 8$/group). ***A***, NVHL reduced the total dendritic length of these neurons and RISP increased it ($^{\alpha}$lesion effect: $p = 0.0047$; $^{\beta}$RISP effect: $p = 0.0221$). ***B***, The dendritic arbor length per branch order analysis showed that the NVHL reduced the length of second and third dendritic orders and RISP reversed it ($^{\alpha}$lesion effect: $p < 0.001$; $^{\beta}$RISP effect: $p < 0.001$; $^{\%}p < 0.01$ vs sham-RISP and NVHL-RISP, $p < 0.001$ vs sham-vehicle; $^{\&}p < 0.001$ vs all the other groups). ***C***, Concerning dendritic spine density, RISP recovered the number of spines lost by the NVHL ($^{\alpha}$lesion effect: $p = 0.039$; $^{\beta}$RISP effect: $p = 0.012$; $^{**}p < 0.01$ vs all the other groups). ***D***, NVHL had differential effects on dendritic spine dynamics, because it reduced the number of mushroom and thin spines and increased the stubby, multi-headed and unclassified spines ($^{\alpha}$lesion effect: mushroom, stubby, multi-headed, and unclassified $p < 0.001$; thin $p = 0.052$; $^{\#}p < 0.01$ vs sham groups, $p < 0.001$ vs NVHL-RISP; $^{***}p < 0.001$ vs all the other groups). RISP decreased the number of stubby spines and increased the rest of the spine populations ($^{\beta}$RISP effect on stubby spines $p = 0.002$, on mushroom spines $p = 0.004$, on thin, bifurcated, multi-headed, and unclassified spines $p < 0.001$). Statistical analyses were conducted using a two-way ANOVA, Newman Keuls *post hoc* test.

15.17, $p < 0.001$; lesion: $F_{(1,28)} = 40.56$, $p < 0.001$; RISP: $F_{(1,28)} = 28.94$, $p < 0.001$); *post hoc* analyses identified that RISP recovered the multi-headed spine population in NVHL animals ($p < 0.001$; Fig. 3*D*). NVHL increased and RISP decreased the number of unclassified spines (lesion: $F_{(1,28)} = 13.69$, $p < 0.001$; RISP: $F_{(1,28)} = 38.02$, $p < 0.001$; Fig. 3*D*).

Regarding PFC layer 5, RISP increased the total dendritic length of these neurons ($F_{(1,28)} = 10.35$, $p = 0.003$) without a NVHL effect ($F_{(1,28)} = 3.077$, $p = 0.09$), also an interaction between factors was almost significant ($F_{(1,28)} = 4.05$, $p = 0.054$); in that sense, *post hoc* analyses were made and revealed that RISP rescued the dendritic length in NVHL animals ($p < 0.05$; Fig. 4*A*). The branch order analysis exposed that NVHL-vehicle rats had reduced the length of the second, third and fourth branch orders (interaction: $F_{(18,196)} = 2.094$, $p = 0.007$; lesion: $F_{(3,196)} = 13.85$, $p < 0.001$; dendritic order: $F_{(6,196)} = 495.0$, $p < 0.001$), and RISP recovered all of them (*post hoc*, second order: $p < 0.05$; third and fourth orders: $p < 0.001$; Fig. 4*B*). Also in this layer, an interaction between lesion and RISP was found in dendritic spine density ($F_{(1,28)} = 13.57$, $p = 0.001$), *post hoc* analyses identified that RISP recovered the spine density in NVHL animals ($p < 0.01$; Fig. 4*C*). Regarding dendritic spine morphological classification, mushroom spine population decreased in NVHL animals ($F_{(1,28)} = 14.2$, $p < 0.001$) and RISP treatment increased these kinds of spines ($F_{(1,28)} = 5.6$, $p = 0.025$), also interaction between factors was almost significant ($F_{(1,28)} = 4.1$, $p = 0.052$; Fig. 4*D*); as such, a *post hoc* test was made and revealed that RISP recovered the number of mushroom spines in the NVHL rats ($p < 0.01$; Fig. 4*D*). The stubby spine population increased because of NVHL and decreased as a RISP effect, but also a significant interaction between lesion and RISP was found (interaction: $F_{(1,28)} = 7.154$, $p = 0.012$; lesion: $F_{(1,28)} = 6.912$, $p = 0.014$; RISP: $F_{(1,28)} = 11.75$, $p = 0.002$); the *post hoc* test identified that RISP recovered the population of these spines in NVHL animals ($p < 0.001$; Fig. 4*D*). There were no NVHL or RISP effects on thin, bifurcated, and multi-headed spines population (Fig. 4*D*). NVHL decreased and RISP increased unclassified spine population (lesion: $F_{(1,28)} = 5.025$, $p = 0.033$; RISP: $F_{(1,28)} = 5.725$, $p = 0.024$; Fig. 4*D*).

Effects of RISP on cell density in the PFC due to NVHL

NVHL reduced the number of cells in the PFC Cg1 area, without RISP effect (lesion: $F_{(1,12)} = 30.43$, $p < 0.001$; RISP: $F_{(1,12)} = 2.745$, $p > 0.05$; Fig. 5*B*).

Effects of NVHL and RISP treatment on neuronal plasticity-associated molecular pathways in the PFC

The brain-derived neurotrophic factor (BDNF) and its interaction with the tropomyosin-receptor-kinase receptor B (TrkB) is implicated in neuronal plasticity. BDNF protein levels remained

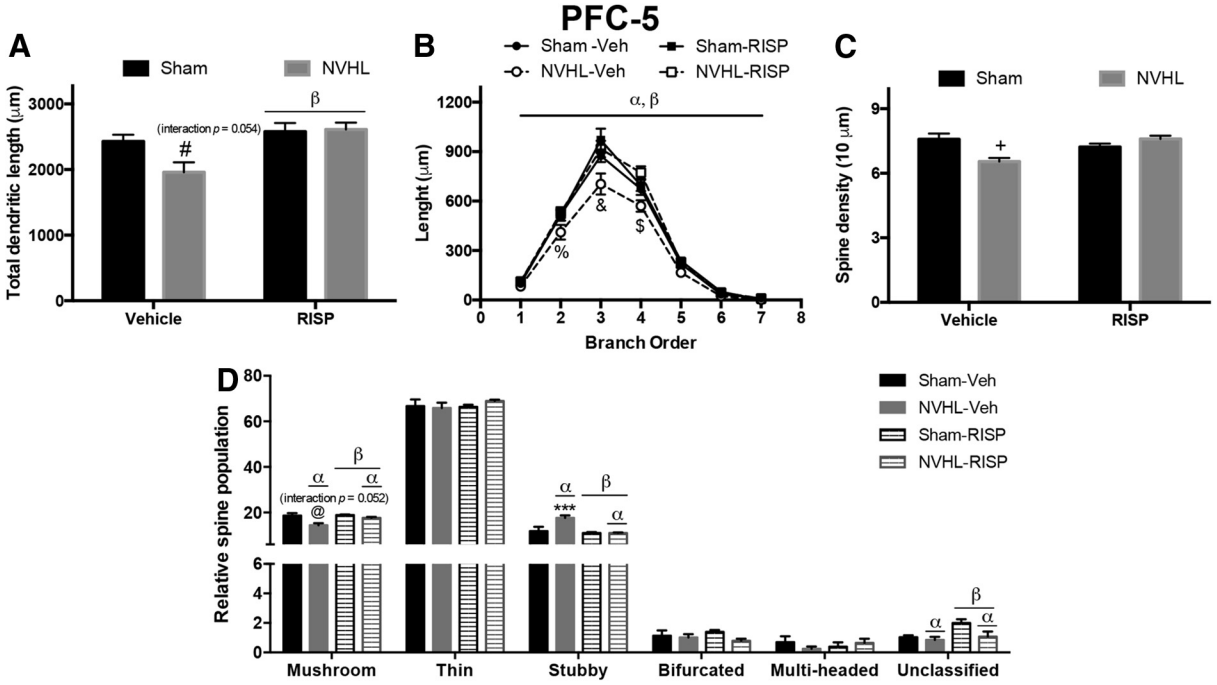

Figure 4. NVHL generates neural atrophy in the PFC layer 5 neurons, which RISP treatment ameliorated ($n = 8$/group). ***A***, RISP increased the total dendritic length of these neurons, and because the interaction between factors was very close to a significant threshold, a *post hoc* test indicated that NVHL animals treated with vehicle had a decreased arbor length that RISP recovered ($^{\beta}$RISP effect: $p = 0.003$; $^{\#}p < 0.05$ vs sham-RISP, $p < 0.01$ vs sham-vehicle and NVHL-RISP). ***B***, Analysis of dendritic arbor length per branch order analysis showed that the NVHL reduced the length of second, third, and fourth dendritic orders and RISP reversed it ($^{\alpha}$lesion effect: $p < 0.001$; $^{\beta}$RISP effect: $p = 0.025$; $^{\%}p < 0.05$ vs all the other groups, $^{\&}p < 0.001$ vs all the other groups; $^{\$}p < 0.05$ vs both sham groups and $p < 0.001$ vs NVHL-RISP). ***C***, Concerning dendritic spine density, RISP recovered the number of spines lost by the NVHL ($^{+}p < 0.05$ vs sham-RISP, $p < 0.01$ vs sham-vehicle and NVHL-RISP). ***D***, NVHL had differential effects on dendritic spine dynamics, since it reduced the number of mushroom and unclassified spines, and RISP increased both populations (mushroom $^{\alpha}$lesion effect: $p < 0.001$; $^{\beta}$RISP effect: $p < 0.001$; unclassified $^{\alpha}$lesion effect: $p = 0.033$; $^{\beta}$RISP effect: $p = 0.024$). Interaction in the mushroom spine population was very close to the significance threshold and *post hoc* analyses indicated that NVHL vehicle-treated animals had fewer mushroom spines that RISP treatment recovered ($^{@}p < 0.01$ vs NVHL-RISP, $p < 0.001$ vs both sham groups). Stubby spine population increased because of NVHL and decreased as RISP effect ($^{\alpha}$lesion effect: $p = 0.014$; $^{\beta}$RISP effect: $p = 0.002$), a *post hoc* test revealed that NVHL vehicle-treated animals had more stubby spines that RISP treatment reduced ($^{***}p < 0.001$ vs all the other groups). Thin, bifurcated, and multi-headed spine populations remained unchanged between groups. Statistical analyses were conducted using a two-way ANOVA, Newman Keuls *post hoc* test.

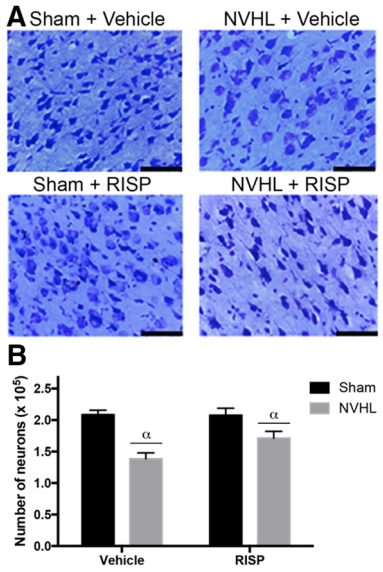

Figure 5. NVHL generate a neural loss in the PFC. ***A***, Representative photomicrographs of cresyl violet-stained brain sections of the region-of-interest. Scale bar, 100 μm. ***B***, NVHL decreased the cell number without a RISP effect ($n = 4$/group; $^{\alpha}$lesion effect: $p < 0.001$). Statistical analyses were conducted using a two-way ANOVA.

unchanged among groups (Fig. 6*A*). Two isoforms of TrkB were analyzed, the full-length one (TrkB-FL), which increased because of RISP ($F_{(1,16)} = 10.36$, $p = 0.005$) and there was a trend of the NVHL to reduce it ($F_{(1,16)} = 4.020$, $p = 0.062$; Fig. 6*B*); and the truncated isoform glycoprotein-95 (TrkB-T1) whose levels remained unchanged (Fig. 6*C*). Also, it was calculated a ratio among TrkB-FL/T1, which increased because of RISP ($F_{(1,16)} = 8.610$, $p = 0.01$) without NVHL effect ($F_{(1,16)} = 0.4302$, $p > 0.05$; Fig. 6*D*). Within the diverse signaling pathway activated by BDNF/TrkB activity, there are phosphoinositide 3-kinase (PI3K)/protein kinase B (Akt) and mitogen-activated protein kinases (MAPK) pathways. PI3K levels decreased in the rats with NVHL ($F_{(1,16)} = 15.92$, $p = 0.001$), and the RISP increased the levels of this protein ($F_{(1,16)} = 16.26$, $p = 0.001$; Fig. 6*E*). Interaction between lesion and RISP was found in Akt ratio ($F_{(1,16)} = 7.932$, $p = 0.012$), which increased in the NVHL-RISP animals only in comparison with the NVHL-vehicle group (*post hoc*: $p < 0.05$; Fig. 6*F*). Moreover, a MAPK pathway involved in neuronal plasticity is the one regulated by the extracellular-regulated kinase (ERK). NVHL has no effect on ERK ratio protein levels ($F_{(1,16)} = 0.4513$; $p > 0.05$), but increased because of RISP ($F_{(1,16)} = 8.889$; $p = 0.009$); also an interaction between lesion and RISP was significant ($F_{(1,16)} = 7.401$, $p = 0.015$) and *post hoc* test analyses showed that RISP recovered the decreased levels of ERK ratio in NVHL animals ($p < 0.01$; Fig. 6*G*).

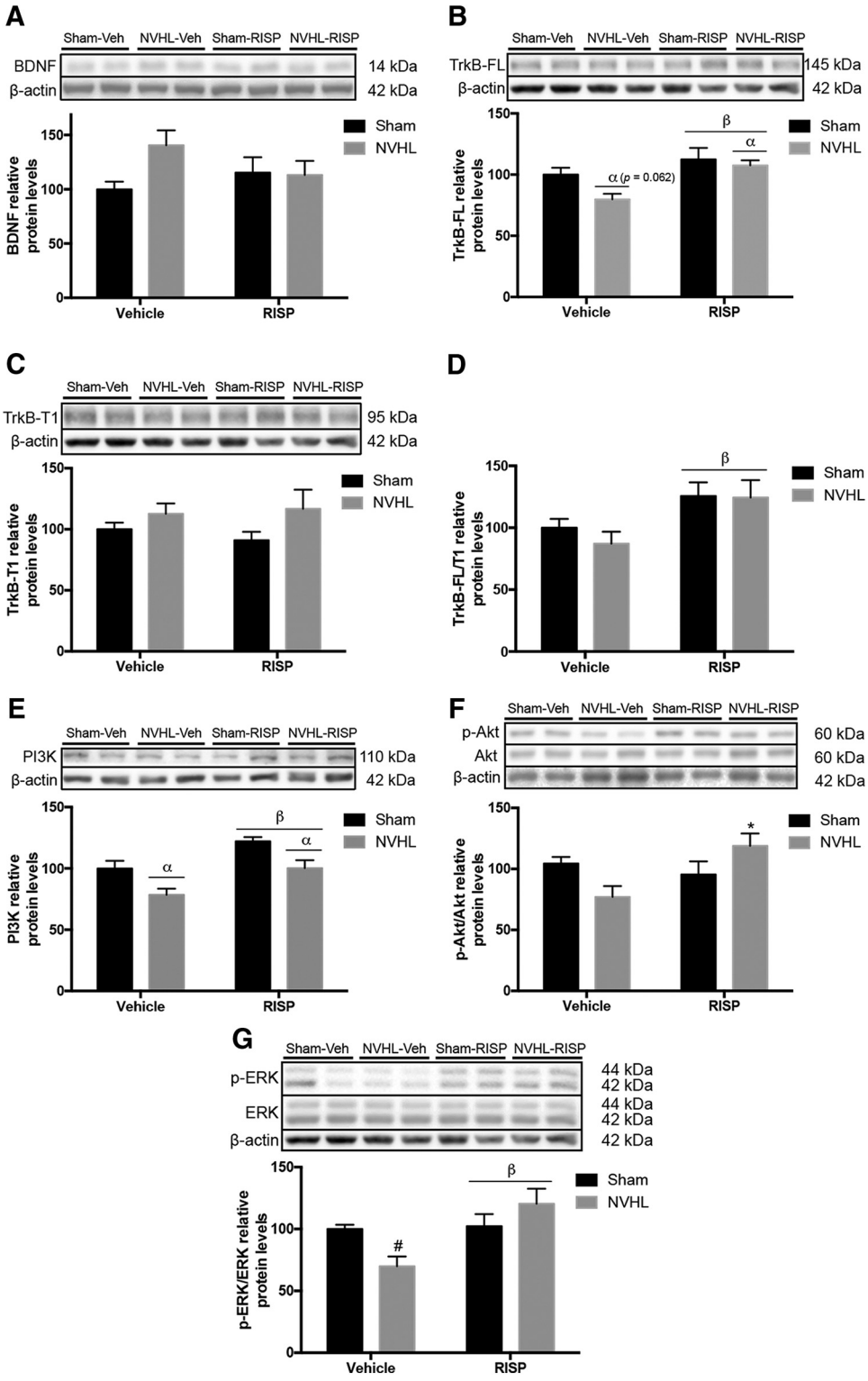

Figure 6. NVHL disrupts the BDNF/TrkB pathway in the PFC. Representative Western blot images of each protein and group ($n = 5$/group). ***A***, BDNF did not change among groups. ***B***, The NVHL effect of reducing TrkB-FL levels was close to significance threshold, however, RISP treatment increased them ($^{\alpha}$lesion effect: $p = 0.062$; $^{\beta}$RISP effect: $p = 0.005$). ***C***, TrkB-T1 remained unchanged among groups. ***D***, TrkB-FL/T1 ratio increased because of RISP ($^{\beta}$RISP effect: $p = 0.001$). ***E***, NVHL reduced PI3K levels and RISP increased them ($^{\alpha}$lesion effect: $p = 0.001$; $^{\beta}$RISP effect: $p = 0.001$). ***F***, Akt increased in the NVHL rats after RISP treatment ($^{*}p < 0.05$ vs NVHL-vehicle). ***G***, RISP increased ERK-ratio levels and recovered the decrease in the NVHL animals ($^{\beta}$RISP effect: $p = 0.009$; $^{\#}p < 0.05$ vs both sham groups, $p < 0.01$ vs NVHL-RISP). Statistical analyses were conducted using a two-way ANOVA, Newman Keuls *post hoc* test.

Effects of NVHL and RISP treatment on inflammatory and oxidative/nitrosative stress markers in the PFC

To evaluate the inflammatory state in the PFC, the nuclear factor-κ B (NF-κB) pathway was studied. The inhibitory subunit of the NF-κB, I κ B α (IκBα), increased because of RISP ($F_{(1,16)} = 8.129$, $p = 0.012$) without NVHL effect ($F_{(1,16)} = 0.1575$, $p > 0.05$; Fig. 7*A*). Neither lesion or RISP treatment affected NF-κB levels (Fig. 7*B*). Also, the cyclooxygenase-2 (COX-2) levels were

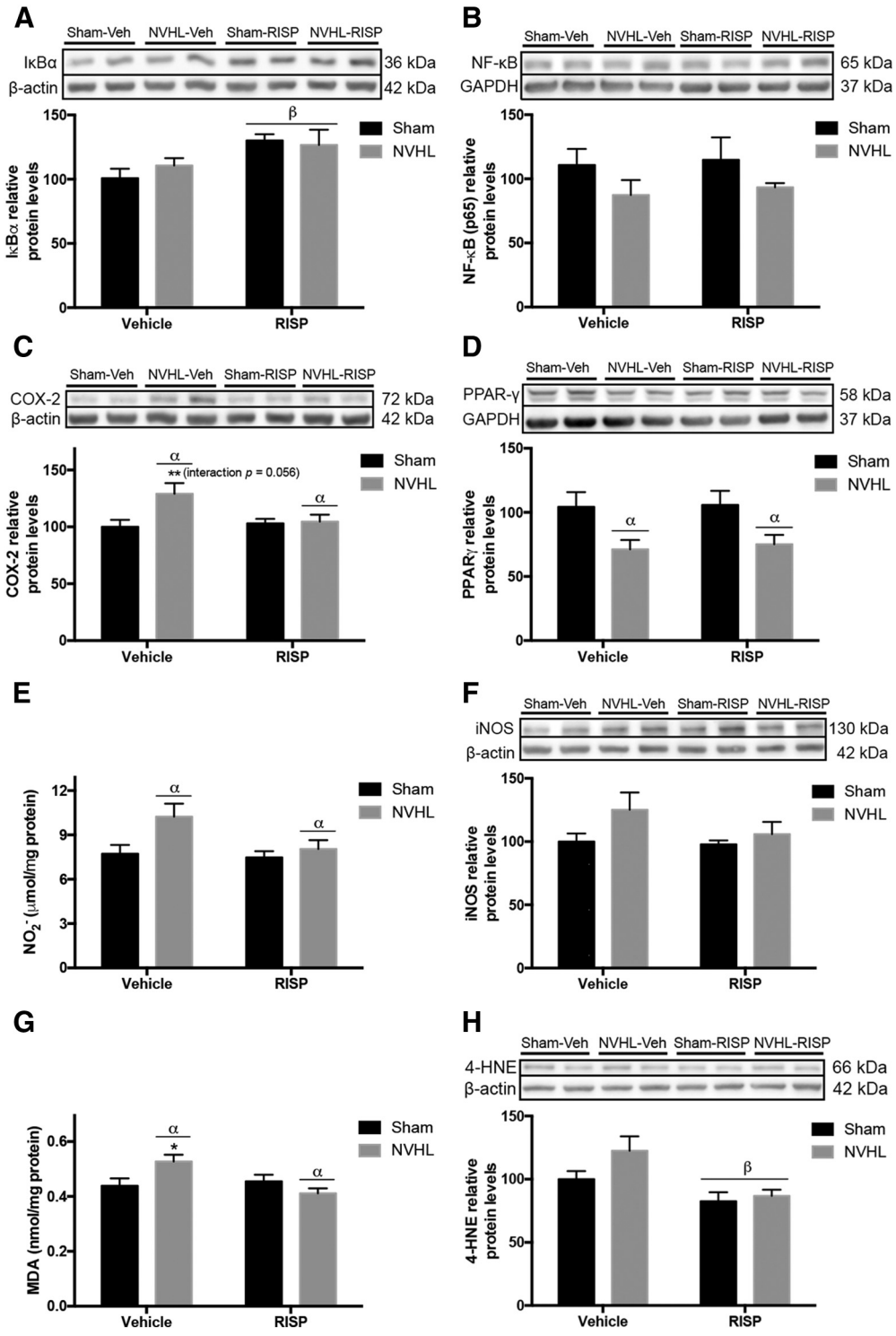

Figure 7. NVHL generates oxidative/nitrosative stress in the PFC, that RISP treatment ameliorates. Representative Western blot images of each protein and group ($n = 5$/group). ***A***, ***B***, The NF-κB pathway was studied and (***A***) RISP increased IκBα levels ($^{\beta}$RISP effect: $p = 0.012$) but (***B***) neither NVHL or RISP had an effect on NF-κB levels. ***C***, COX-2 increased as a consequence of NVHL and because the interaction between factors was very close to the significance threshold a *post hoc* test was made and revealed that RISP reduced COX-2 levels in the NVHL animals ($^{\alpha}$lesion effect: $p = 0.035$; $^{**}p < 0.01$ vs all the other groups). ***D***, NVHL reduced PPAR-γ protein levels ($^{\alpha}$lesion effect: $p = 0.004$). ***E***, NVHL increased NO_2^- concentration ($^{\alpha}$lesion effect: $p = 0.03$). ***F***, iNOS levels remained without changes among experimental groups. ***G***, NVHL increased MDA concentration, *post hoc* analyses revealed that MDA concentration decreased because of RISP in NVHL animals ($^{\alpha}$lesion effect: $p = 0.012$; $^{*}p < 0.05$ vs all the other groups). ***H***, RISP reduced the 4-HNE levels ($^{\beta}$RISP effect: $p = 0.004$). Statistical analyses were conducted using a two-way ANOVA, Newman Keuls *post hoc* test.

evaluated, which increased as the main effect of the NVHL ($F_{(1,16)} = 5.278$, $p = 0.035$) and interaction between lesion and RISP was almost significant ($F_{(1,16)} = 4.226$, $p = 0.056$; Fig. 7*C*), in that sense, a *post hoc* test was made and COX-2 levels increased only in NVHL-vehicle group ($p < 0.01$), thus RISP reduced COX-2 in NVHL animals. Furthermore, the peroxisome proliferator-activated receptor gamma (PPARγ) protein levels were evaluated, which decreased because of the NVHL ($F_{(1,16)} = 11.34$,

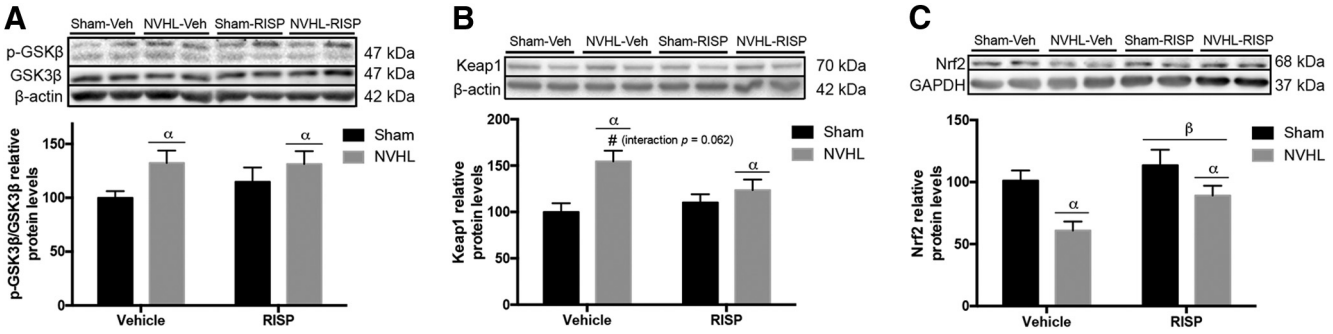

Figure 8. NVHL impairs the Nrf2 pathway in the PFC of NVHL rats ($n = 5$/group). ***A***, NVHL increased GSK-3β levels ($^{\alpha}$lesion effect: $p = 0.04$). ***B***, Also NVHL increased Keap1 protein levels, and because the interaction between factors was very close to significance threshold, a *post hoc* test was made and revealed that RISP decreased Keap1 levels in NVHL animals ($^{\alpha}$lesion effect: $p = 0.005$; $^{\#}p < 0.05$ vs RISP-treated groups and $p < 0.01$ vs sham-vehicle). ***C***, NVHL reduced Nrf2 levels and RISP increased them ($^{\alpha}$lesion effect: $p = 0.003$; $^{\beta}$RISP effect: $p = 0.04$). Statistical analyses were conducted using a two-way ANOVA, Newman Keuls *post hoc* test.

$p = 0.004$) and RISP did not affect ($F_{(1,16)} = 0.08502$, $p > 0.05$; Fig. 7*D*).

To explore oxidative/nitrosative stress, NO_2^- concentration was examined. NVHL animals had higher NO_2^- levels ($F_{(1,16)} = 5.689$, $p = 0.029$), without RISP effect ($F_{(1,16)} = 3.543$, $p = 0.078$; Fig. 7*E*). Then, neither NVHL or RISP affected the inducible isoform of the nitric oxide synthase (iNOS) levels (Fig. 7*F*). Also, lipid peroxidation markers MDA and 4-hydroxy-2-nonenal (4-HNE) were evaluated. NVHL has no effect on MDA concentration ($F_{(1,16)} = 9.021$, $p > 0.05$) but RISP decreased it ($F_{(1,16)} = 4.592$, $p = 0.048$), and the interaction between the lesion and RISP was significant ($F_{(1,16)} = 8.106$, $p = 0.012$); the *post hoc* test indicated that RISP reduced the concentration of MDA in NVHL animals ($p < 0.05$; Fig. 7*G*). Moreover, RISP decreased 4-HNE protein levels ($F_{(1,16)} = 11.61$, $p = 0.004$) without the NVHL effect ($F_{(1,16)} = 2.953$, $p > 0.105$; Fig. 7*H*).

Regarding the nuclear factor (erythroid-derived 2)-like 2 (Nrf2) pathway, which is related to the antioxidant response was evaluated. The glycogen synthase kinase 3 β (GSK-3β) modulates the activity of the Kelch-like ECH-associated protein 1 (Keap1), which is the cytosolic inhibitor of Nrf2. NVHL increased GSK-3β ratio ($F_{(1,16)} = 4.975$, $p = 0.04$) and RISP did not modify this ratio ($F_{(1,16)} = 0.3938$, $p > 0.05$; Fig. 8*A*). The same patter effect was observed in Keap1 protein levels, which increased in NVHL animals ($F_{(1,16)} = 10.79$, $p = 0.005$) without RISP effect ($F_{(1,16)} = 1.012$, $p > 0.05$); and because the interaction between factors was close significance threshold ($F_{(1,16)} = 3.999$, $p = 0.063$; Fig. 8*B*), a *post hoc* test was made and revealed that RISP reduced Keap1 levels in NVHL animals ($p < 0.01$). Finally, NVHL decreased the nuclear protein levels of Nrf2 and RISP increased them (lesion: $F_{(1,16)} = 12.53$, $p = 0.003$; RISP: $F_{(1,16)} = 4.937$, $p = 0.041$; Fig. 8*C*).

Effects of NVHL and RISP treatment on inflammatory and oxidative/nitrosative stress markers in serum and PBMCs

The peripheral inflammatory balance was evaluated in PBMC. Regarding the NF-κB pathway, the NVHL did not change IκBα levels ($F_{(1,16)} = 0.00249$, $p > 0.05$), but RISP treatment increased them ($F_{(1,16)} = 9.167$, $p = 0.008$; Fig. 9*A*). However, NF-κB protein levels remained unchanged (Fig. 9*B*). Both NVHL and RISP increased COX-2 protein levels (lesion: $F_{(1,16)} = 4.766$, $p = 0.044$; RISP: $F_{(1,16)} = 9.601$, $p = 0.007$; Fig. 9*C*). PPARγ protein levels remained unchanged among groups (Fig. 9*D*). Also NO_2^- and iNOS was explored. NVHL increased NO_2^- concentration ($F_{(1,16)} = 4.703$, $p = 0.045$) without RISP effect ($F_{(1,16)} = 0.0878$, $p > 0.05$; Fig. 9*E*). For iNOS levels, there was an interaction between lesion and RISP factors ($F_{(1,16)} = 4.835$, $p = 0.043$; Fig. 9*F*), however, no differences among groups were significant. Interaction between lesion and RISP was close to the significance threshold for MDA concentration ($F_{(1,16)} = 4.042$, $p = 0.061$), in that sense, the *post hoc* test revealed that RISP reduced MDA concentration in NVHL animals ($p < 0.05$; Fig. 9*G*). 4-HNE showed an interaction between factors ($F_{(1,16)} = 7.805$, $p = 0.013$) and RISP treatment decreased the protein levels only in the NVHL rats (*post hoc*: $p < 0.05$; Fig. 9*H*). Finally, regarding the Nrf2 pathway, NVHL increased GSK-3β ratio levels ($F_{(1,16)} = 5.839$, $p = 0.028$) and significant interaction between lesion and RISP was found ($F_{(1,16)} = 5.455$, $p = 0.033$), RISP recovered GSK-3β ratio in the NVHL animals (*post hoc*: $p < 0.05$; Fig. 10*A*). However, Keap1 protein levels did not change (Fig. 10*B*). NVHL was closely to be significant as the main effect promoting the increase of Nrf2 protein levels ($F_{(1,16)} = 3.959$, $p = 0.064$) and RISP did not affect them ($F_{(1,16)} = 2.301$, $p > 0.05$; Fig. 10*C*).

Discussion

We found that NVHL rats have dendritic arbor and spine pathology in pyramidal cells of the PFC when studied at adulthood. Also, these animals lose cells due to impaired BDNF/TrkB signaling and oxidative/nitrosative stress in this area. Furthermore, adult animals subjected to NVHL exhibit peripheral oxidative/nitrosative stress. Twenty-one consecutive days of RISP treatment (0.25 mg/kg, i.p.) ameliorated most of those alterations and also corrected behavioral abnormalities observed in the NVHL rats.

PFC dysfunction is associated with the behavioral alterations exhibited by the NVHL rats (O'Donnell, 2012). The novel environment hyperlocomotion of NVHL animals is related to stress vulnerability observed in schizophrenia, and indicates an increase in the ventral striatum dopaminergic tone (Flores et al., 1996, 2005). Therefore, RISP reduced mesolimbic dopaminergic hyperfunction in rats with NVHL, and as a consequence the number of movements during the motor test. Also, the rise in the ventral striatum dopaminergic tone generates a dysregulation in the corticolimbic system due to NAcc GABAergic hyperactivity in the ventral pallidum. This structure regulates the spontaneous activity of the dorsomedial thalamus, and the aforementioned would dysregulate the PFC function (Flores et al., 2016). Also, NVHL rats had poor social interaction, an innate behavior in the rats (Vanderschuren et al., 1997) that can be related to social isolation, a negative symptom of SZ (Wible et al., 2001). Generally, negative symptoms only improve with long antipsychotic treatments (Remington et al., 2016). In our study, RISP only

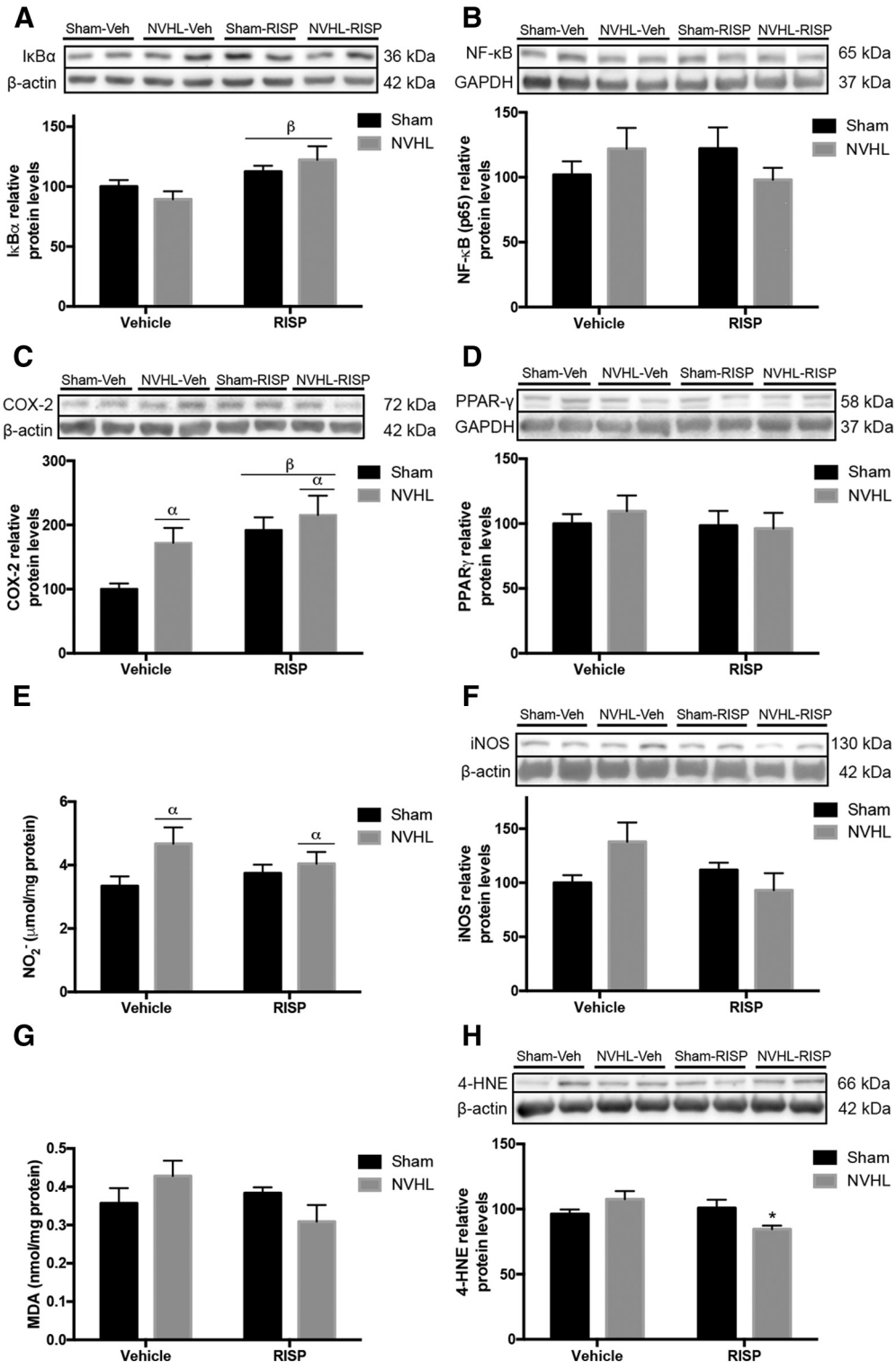

Figure 9. Oxidative/nitrosative stress was observed in the periphery of NVHL rats ($n = 5$/group). ***A***, IκBα increased after RISP treatment ($^{\beta}$RISP effect: $p = 0.008$). ***B***, NF-κB levels remained unchanged. ***C***, COX-2 increased as a consequence of NVHL and RISP treatment ($^{\beta}$RISP effect: $p = 0.008$). ***D***, PPAR-γ protein levels remained unchanged. ***E***, NO_2^- concentration increased because of NVHL ($^{\alpha}$lesion effect: $p = 0.045$). ***F***, iNOS protein levels, as well as (***G***) MDA concentration remained unchanged among experimental groups. ***H***, RISP reduced the 4-HNE protein levels in NVHL animals (*$p < 0.05$ vs NVHL-vehicle). Statistical analyses were conducted using a two-way ANOVA, Newman Keuls *post hoc* test.

improved the number of social encounters of NVHL animals, may be because of the duration of the treatment.

Behavioral enhancement as a result of RISP in NVHL rats might have functional and anatomical substrates at the CNS level. Our results demonstrate that PFC pyramidal neurons of NVHL animals are atrophied and have a dendritic spine pathology and RISP treatment ameliorated those morphological alterations.

Neural plasticity is regulated by various molecules, including neurotrophic factors such as BDNF. BDNF acts via Trk receptors,

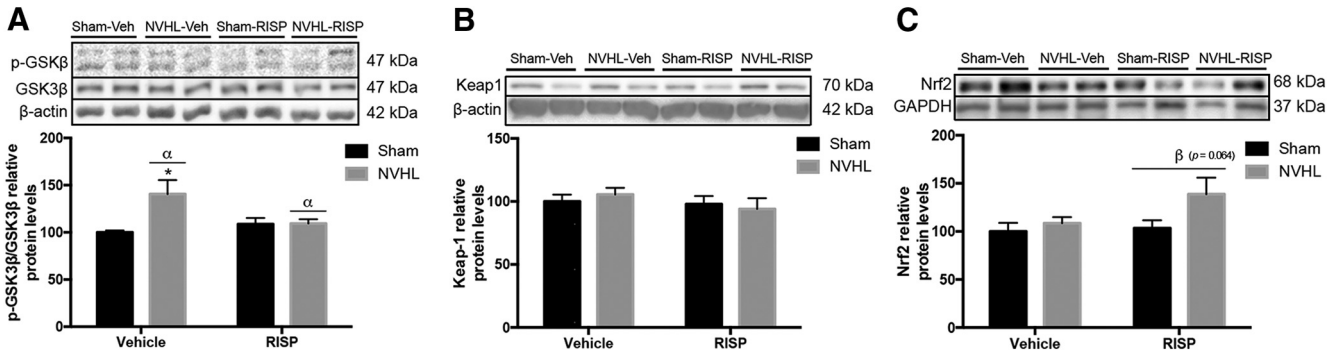

Figure 10. Evaluation of the Nrf2 pathway in PBMC of NVHL rats ($n = 5$/group). ***A***, GSK-3β ratio levels increased in NVHL animals and RISP treatment reduced them in these rats ($^{\alpha}$lesion effect: $p = 0.028$; $^{*}p < 0.05$ vs all the other groups). ***B***, Keap1 protein levels remained unchanged among groups. ***C***, The RISP effect of increasing Nrf2 protein levels was close to the significance threshold ($^{\beta}$RISP effect: $p = 0.064$). Statistical analyses were conducted using a two-way ANOVA, Newman Keuls *post hoc* test.

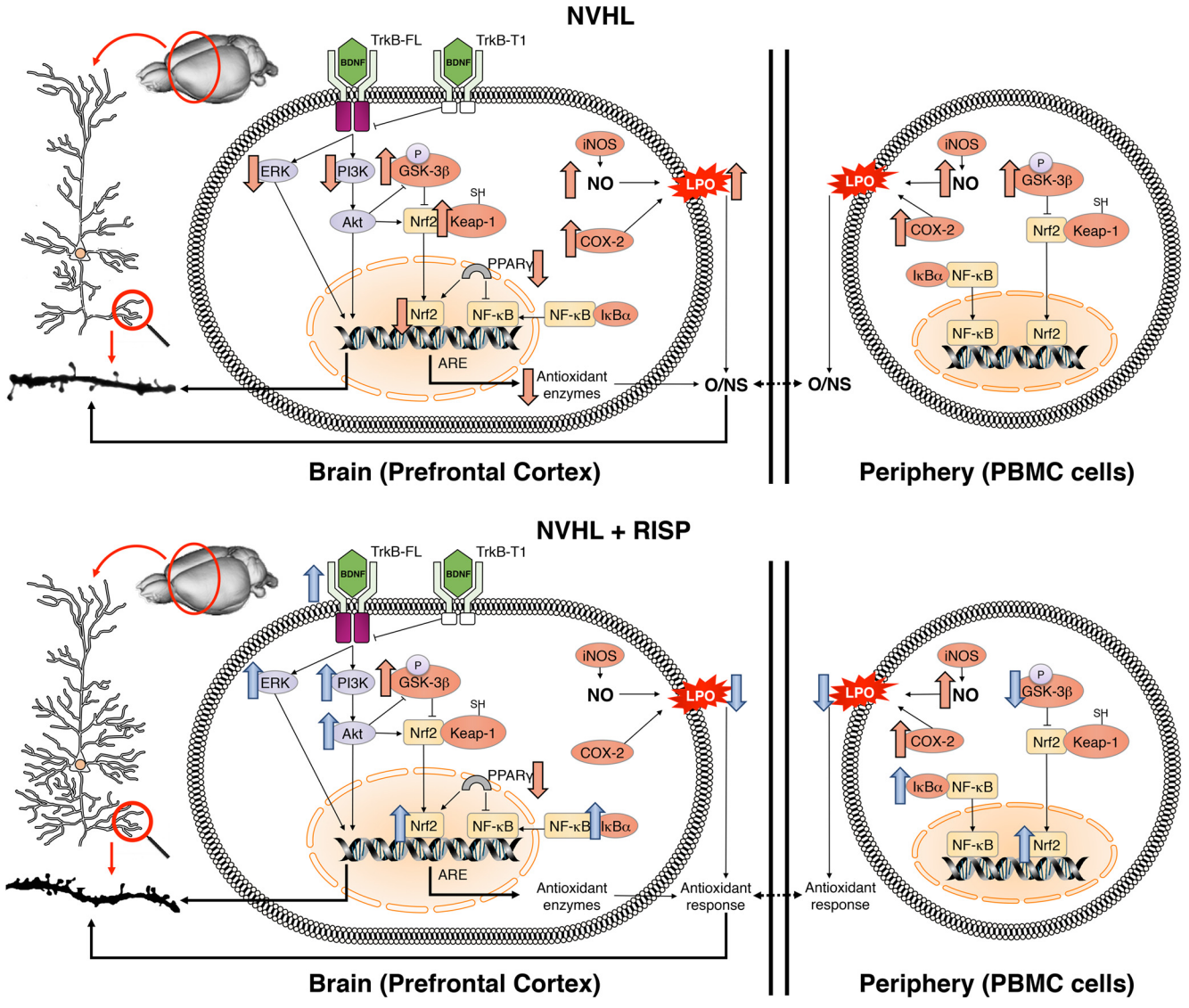

Figure 11. Schematic abstract of the results. BDNF/TrkB pathway is disrupted in the PFC of NVHL animals as well as the downstream ERK and PI3K/Akt pathways. Also, increased NO_2^-, COX-2 and impaired Nrf2 pathway results in lipid peroxidation (LPO) and oxidative/nitrosative stress. The aforementioned is related to neural atrophy and the dendritic spine pathology in PFC pyramidal cells. RISP had neurotrophic and antioxidant effects restoring BDNF/TrkB and Nrf2 pathways, respectively, and ultimately ameliorated morphological impairments in the PFC. Oxidative/nitrosative stress can also be detected in the periphery of NVHL rats, and a COX-2 increase was observed both in the PFC and in the PBMC. RISP reduced LPO but increased COX-2 levels in sham animals.

and the most abundant isoform in the neocortex is the TrkB, including the TrkB-FL and TrkB-T1 isoforms (Middlemas et al., 1991; Bramham and Messaoudi, 2005). When BDNF interacts with TrkB-FL, it promotes the arborization of the dendritic arbor and spinogenesis (Cohen-Cory et al., 2010); but when it interacts with TrkB-T1 it has an antagonistic effect on TrkB-FL signaling (Carim-Todd et al., 2009). Neither BDNF, TrkB-FL, and TrkB-T1 were affected by NVHL. However, RISP increased the TrkB-FL levels in the NVHL rats. Interestingly, a reduction in BDNF mRNA in the PFC of NVHL animals has been observed (Lipska et al., 2001).

Alterations in the counterbalancing effect of TrkB-FL and TrkB-T1, assessed by the ratio of TrkB-FL to TrkB-T1 expression (hereafter FL/T1 ratio), have been used as a variable index for describing BDNF receptor expression and has been related to distinct mental disorders (Fenner, 2012), including SZ (Wong et al., 2013; Martinez-Cengotitabengoa et al., 2016). RISP treatment increased the TrkB FL/T1 ratio in both sham and NVHL rats.

BDNF/TrkB activity stimulates ERK and PI3K/Akt pathways, which represent a potential therapeutic target of much interest in several mental illnesses, such as SZ (Alonso et al., 2004; Yuan et al., 2010; Enriquez-Barreto and Morales, 2016). Phosphorylated ERK immunoreactivity develops rapidly in dendritic regions in long-term potentiation (LTP) phenomena (Dudek and Fields, 2001; Kelleher et al., 2004; Tang and Yasuda, 2017), a cellular substrate for cognitive functions (Ying et al., 2002). For LTP development, an adequate quantity, composition and spatial disposition of postsynaptic density (PSD) are necessary (Bosch et al., 2014; Nicoll, 2017). The PSD is made of several cytoskeleton-related proteins, adhesion molecules, and receptors, including TrkB (Aoki et al., 2000; Sheng and Hoogenraad, 2007). As the PSD is specifically located on the spine surface, its expansion results in a bigger head size. In such a manner, there is a correlation between shape and function in the dendritic spines, the mushroom-shaped spines being considered mature spines (Matsuzaki et al., 2004). Thus, ERK activity is not only associated with dendritic spine synaptic function but also novel spine formation and maturation (Tang and Yasuda, 2017). Here we demonstrate that NVHL attenuates ERK in the PFC as demonstrated before (Bychkov et al., 2011), and this could be related to the lack of spines, as well as the reduction of mature spines in PFC neurons.

Increased PI3K/Akt protein levels were also observed in NVHL animals after RISP treatment. The PI3K/Akt pathway is involved in cell survival (Cardone et al., 1998; Lee et al., 2008), and it's impaired activity described here can be associated with the neural density reduction observed in the NVHL. Although a specific neural population decrease was not studied, because cresyl violet stain only allows us to distinguish between neurons and glia because of their size, a decrease of parvalbumin GABAergic interneurons in the PFC has been demonstrated in the NVHL (Cabungcal et al., 2014). Another factor that can be implicated in the PFC cell loss is oxidative/nitrosative stress.

PI3K/Akt (effector), as well as GSK-3β (inhibitor), regulates the Nrf2 antioxidant pathway (Sandberg et al., 2014). Nrf2 is a nuclear factor that promotes the synthesis of different enzymes, such as glutathione peroxidase and catalase that protects the cells from oxidative/nitrosative stress, and its dysfunction has been reported in SZ (Genc and Genc, 2009). Interestingly, the gene expression of the afore-mentioned enzymes is reduced in the NVHL (Hui et al., 2019), in congruence with the disruption of the Nrf2 pathway reported here. This impaired antioxidant response could promote oxidative/nitrosative stress. In such a manner, we analyze the nitric oxide (NO) system by quantifying NO_2^- levels as well as the iNOS (Guix et al., 2005). Here we found that NVHL animals have increased NO_2^- levels in the PFC, in congruence with previous reports (Negrete-Díaz et al., 2010; Bringas et al., 2012), however, the source of this NO_2^- rise has not been examined yet. iNOS is overexpressed in glial cells in response to inflammatory stimuli and produces a large amount of NO (Galea et al., 1992). NVHL does not have an effect on iNOS protein levels, suggesting that other molecules are implicated in oxidative/nitrosative stress.

COX-2 is a potent inflammatory mediator that activates microglia, and the levels of this protein increased in the NVHL animals (Garden and Möller, 2006). Excessive microglia population and activity has recently been demonstrated in the PFC of NVHL animals (Hui et al., 2019). Thus, it can be proposed that oxidative/nitrosative stress is modulated by microglia in the NVHL. Interestingly, increased microglia activity also can be related to excessive synapse elimination and postsynaptic spine shape modifications (Weinhard et al., 2018), explaining the reduction of mature spines in the NVHL.

Most of the information about inflammation and oxidative/nitrosative stress in SZ is from plasma or PBMC studies. These findings attempt to explore (indirectly) the inflammatory state of the brain and to find biomarkers for the disease (Miller et al., 2011; Fraguas et al., 2017). We analyzed the peripheral inflammation and oxidative/nitrosative stress in the NVHL model. PBMCs of NVHL animals have increased COX-2 protein levels, a common finding between the brain and periphery. COX-2 inhibits the synthesis of 15-deoxy-delta-12,14-prostaglandin J_2 (15d-PGJ_2) and therefore reduces the anti-inflammatory response via PPARγ. Clinical studies have demonstrated that the reduction in 15d-PGJ_2, a potent anti-inflammatory molecule, and the increase in NF-κB activity are associated with SZ (García-Bueno et al., 2014b). Also, the capacity of RISP has been shown to reduce some proinflammatory cytokines after lipopolysaccharide stimulus (Chen et al., 2012; Al-Amin et al., 2013). Interestingly, RISP increased COX-2 levels in sham and lesioned animals. This can be related to the capability of RISP to increase membrane omega-3 fatty acid synthesis in erythrocytes and the PFC, contributing to an antioxidant effect (McNamara et al., 2009, 2011). Thus, further studies must detail the effects of RISP on PBMCs. However, the antioxidant capacity of RISP was revealed in the NVHL, because it was capable of reducing lipid peroxidation in the PFC and in PBMCs.

In that sense, aforementioned neurotrophic and antioxidant effects could be common antipsychotic mechanisms that ultimately improve behavioral abnormalities in the NVHL model (Rueter et al., 2004; Negrete-Díaz et al., 2010; Bringas et al., 2012). A schematic abstract of the results is shown in Figure 11.

In conclusion, RISP ameliorates neural PFC abnormalities caused by the NVHL not only due to its monoaminergic antagonist activity, but also by restoring plasticity and reducing the oxidative/nitrosative stress. Then, PFC function improves and, as a consequence, the behavior of the animals improve. Moreover, brain inflammatory imbalances and oxidative/nitrosative stress exhibited in the PFC of NVHL animals, and the RISP modulation in these animals, have an association with peripheral markers. This establishes the usefulness of this animal model to explore a linkage between neurodevelopmental and immunological cues relevant for SZ pathophysiology.

References

Al-Amin MM, Nasir Uddin MM, Mahmud Reza H (2013) Effects of antipsychotics on the inflammatory response system of patients with

schizophrenia in peripheral blood mononuclear cell cultures. Clin Psychopharmacol Neurosci 11:144–151.
Alonso M, Medina JH, Pozzo-Miller L (2004) ERK1/2 activation is necessary for BDNF to increase dendritic spine density in hippocampal CA1 pyramidal neurons. Learn Mem 11:172–178.
Alquicer G, Silva-Gómez AB, Peralta F, Flores G (2004) Neonatal ventral hippocampus lesion alters the dopamine content in the limbic regions in postpubertal rats. Int J Dev Neurosci 22:103–111.
Alquicer G, Morales-Medina JC, Quirion R, Flores G (2008) Postweaning social isolation enhances morphological changes in the neonatal ventral hippocampal lesion rat model of psychosis. J Chem Neuroanat 35: 179–187.
Andreazza AC, Shao L, Wang JF, Young LT (2010) Mitochondrial complex I activity and oxidative damage to mitochondrial proteins in the prefrontal cortex of patients with bipolar disorder. Arch Gen Psychiatry 67:360–368.
Andreazza AC, Wang JF, Salmasi F, Shao L, Young LT (2013) Specific subcellular changes in oxidative stress in prefrontal cortex from patients with bipolar disorder. J Neurochem 127:552–561.
Aoki C, Wu K, Elste A, Len Gw, Lin Sy, McAuliffe G, Black IB (2000) Localization of brain-derived neurotrophic factor and TrkB receptors to postsynaptic densities of adult rat cerebral cortex. J Neurosci Res 59:454–463.
Bello-Medina PC, Flores G, Quirarte GL, McGaugh JL, Prado Alcalá RA (2016) Mushroom spine dynamics in medium spiny neurons of dorsal striatum associated with memory of moderate and intense training. Proc Natl Acad Sci U S A 113:E6516–E6525.
Bosch M, Castro J, Saneyoshi T, Matsuno H, Sur M, Hayashi Y (2014) Structural and molecular remodeling of dendritic spine substructures during long-term potentiation. Neuron 82:444–459.
Bradford MM (1976) A rapid and sensitive method for the quantitation of microgram quantities of protein utilizing the principle of protein-dye binding. Analyt Biochem 72:248–254.
Bramham CR, Messaoudi E (2005) BDNF function in adult synaptic plasticity: the synaptic consolidation hypothesis. Prog Neurobiol 76:99–125.
Bringas ME, Morales-Medina JC, Flores-Vivaldo Y, Negrete-Diaz JV, Aguilar-Alonso P, León-Chávez BA, Lazcano-Ortiz Z, Monroy E, Rodríguez-Moreno A, Quirion R, Flores G (2012) Clozapine administration reverses behavioral, neuronal, and nitric oxide disturbances in the neonatal ventral hippocampus rat. Neuropharmacology 62:1848–1857.
Brinholi FF, Farias CC, Bonifácio KL, Higachi L, Casagrande R, Moreira EG, Barbosa DS (2016) Clozapine and olanzapine are better antioxidants than haloperidol, quetiapine, risperidone and ziprasidone in *in vitro* models. Biomed Pharmacother 81:411–415.
Brusco J, Dall'Oglio A, Rocha LB, Rossi MA, Moreira JE, Rasia-Filho AA (2010) Descriptive findings on the morphology of dendritic spines in the rat medial amygdala. Neurosci Lett 483:152–156.
Bychkov E, Ahmed MR, Gurevich EV (2011) Sex differences in the activity of signalling pathways and expression of G-protein-coupled receptor kinases in the neonatal ventral hippocampal lesion model of schizophrenia. Int J Neuropsychopharmacol 14:1–15.
Cabungcal JH, Counotte DS, Lewis E, Tejeda HA, Piantadosi P, Pollock C, Calhoon GG, Sullivan E, Presgraves E, Kil J, Hong LE, Cuenod M, Do KQ, O'Donnell P (2014) Juvenile antioxidant treatment prevents adult deficits in a developmental model of schizophrenia. Neuron 83:1073–1084.
Cardone MH, Roy N, Stennicke HR, Salvesen GS, Franke TF, Stanbridge E, Frisch S, Reed JC (1998) Regulation of cell death protease caspase-9 by phosphorylation. Science 282:1318–1321.
Carim-Todd L, Bath KG, Fulgenzi G, Yanpallewar S, Jing D, Barrick CA, Becker J, Buckley H, Dorsey SG, Lee FS, Tessarollo L (2009) Endogenous truncated TrkB.T1 receptor regulates neuronal complexity and TrkB kinase receptor function *in vivo*. J Neurosci 29:678–685.
Castellano O, Arji M, Sancho C, Carro J, Riolobos AS, Molina V, Gómez-Nieto R, de Anchieta de Castro E Horta J Jr, Herrero-Turrión MJ, López DE (2013) Chronic administration of risperidone in a rat model of schizophrenia: a behavioural, morphological and molecular study. Behav Brain Res 242:178–190.
Chareyron LJ, Lavenex PB, Lavenex P (2012) Postnatal development of the amygdala: a stereological study in rats. J Comp Neurol 520:3745–3763.
Chen SL, Lee SY, Chang YH, Chen SH, Chu CH, Tzeng NS, Lee IH, Chen PS, Yeh TL, Huang SY, Yang YK, Lu RB, Hong JS (2012) Inflammation in patients with schizophrenia: the therapeutic benefits of risperidone plus add-on dextromethorphan. J Neuroimmune Pharmacol 7:656–664.
Cohen-Cory S, Kidane AH, Shirkey NJ, Marshak S (2010) Brain-derived neurotrophic factor and the development of structural neuronal connectivity. Dev Neurobiol 70:271–288.
Das NP, Ratty AK (1987) Studies on the effects of the narcotic alkaloids, cocaine, morphine, and codeine on nonenzymatic lipid peroxidation in rat brain mitochondria. Biochem Med Metab Biol 37:258–264.
Dickerson F, Stallings C, Origoni A, Schroeder J, Katsafanas E, Schweinfurth L, Savage C, Khushalani S, Yolken R (2016) Inflammatory markers in recent onset psychosis and chronic schizophrenia. Schizophr Bull 42:134–141.
Dudek SM, Fields RD (2001) Mitogen-activated protein kinase/extracellular signal-regulated kinase activation in somatodendritic compartments: roles of action potentials, frequency, and mode of calcium entry. J Neurosci 21:RC122.
Enriquez-Barreto L, Morales M (2016) The PI3K signaling pathway as a pharmacological target in autism related disorders and schizophrenia. Mol Cell Ther 4:2.
Fenner BM (2012) Truncated TrkB: beyond a dominant negative receptor. Cytokine Growth Factor Rev 23:15–24.
File SE (1980) The use of social interaction as a method for detecting anxiolytic activity of chlordiazepoxide-like drugs. J Neurosci Methods 2:219–238.
Flores G, Barbeau D, Quirion R, Srivastava LK (1996) Decreased binding of dopamine D3 receptors in limbic subregions after neonatal bilateral lesion of rat hippocampus. J Neurosci 16:2020–2026.
Flores G, Alquicer G, Silva-Gómez AB, Zaldivar G, Stewart J, Quirion R, Srivastava LK (2005) Alterations in dendritic morphology of prefrontal cortical and nucleus accumbens neurons in post-pubertal rats after neonatal excitotoxic lesions of the ventral hippocampus. Neuroscience 133: 463–470.
Flores G, Morales-Medina JC, Diaz A (2016) Neuronal and brain morphological changes in animal models of schizophrenia. Behav Brain Res 301: 190–203.
Fraguas D, Díaz-Caneja CM, Ayora M, Hernandez-Alvarez F, Rodríguez-Quiroga A, Recio S, Leza JC, Arango C (2017) Oxidative stress and inflammation in first-episode psychosis: a systematic review and meta-analysis. Int J Neuropsychopharmacol 20:435–444.
Galea E, Feinstein DL, Reis DJ (1992) Induction of calcium-independent nitric oxide synthase activity in primary rat glial cultures. Proc Natl Acad Sci U S A 89:10945–10949.
García-Bueno B, Bioque M, MacDowell KS, Santabárbara J, Martínez-Cengotitabengoa M, Moreno C, Sáiz PA, Berrocoso E, Gassó P, Fe Barcones M, González-Pinto A, Parellada M, Bobes J, Micó JA, Bernardo M, Leza JC, Flamm-Peps study CdIBeRdSMS (2014a) Pro-/antiinflammatory dysregulation in early psychosis: results from a 1-year follow-up study. Int J Neuropsychopharmacol 18:pyu037.
García-Bueno B, Bioque M, Mac-Dowell KS, Barcones MF, Martínez-Cengotitabengoa M, Pina-Camacho L, Rodriguez-Jimenez R, Sáiz PA, Castro C, Lafuente A, Santabárbara J, González-Pinto A, Parellada M, Rubio G, García-Portilla MP, Micó JA, Bernardo M, Leza JC (2014b) Pro-/anti-inflammatory dysregulation in patients with first episode of psychosis: toward an integrative inflammatory hypothesis of schizophrenia. Schizophr Bull 40:376–387.
García-Bueno B, Gassó P, MacDowell KS, Callado LF, Mas S, Bernardo M, Lafuente A, Meana JJ, Leza JC (2016) Evidence of activation of the toll-like receptor-4 proinflammatory pathway in patients with schizophrenia. J Psychiatry Neurosci 41:E46–E55.
Garden GA, Möller T (2006) Microglia biology in health and disease. J Neuroimmune Pharmacol 1:127–137.
Garey LJ, Ong WY, Patel TS, Kanani M, Davis A, Mortimer AM, Barnes TR, Hirsch SR (1998) Reduced dendritic spine density on cerebral cortical pyramidal neurons in schizophrenia. J Neurol Neurosurg Psychiatry 65: 446–453.
Genc K, Genc S (2009) Oxidative stress and dysregulated Nrf2 activation in the pathogenesis of schizophrenia. Biosci Hypotheses 2:16–18.
Gibb R, Kolb B (1998) A method for vibratome sectioning of golgi-cox stained whole rat brain. J Neurosci Methods 79:1–4.
Glantz LA, Lewis DA (2000) Decreased dendritic spine density on prefrontal cortical pyramidal neurons in schizophrenia. Arch Gen Psychiatry 57:65–73.
Glausier JR, Lewis DA (2013) Dendritic spine pathology in schizophrenia. Neuroscience 251:90–107.

Green LC, Wagner DA, Glogowski J, Skipper PL, Wishnok JS, Tannenbaum SR (1982) Analysis of nitrate, nitrite, and [^{15}N]nitrate in biological fluids. Anal Biochem 126:131–138.

Guix FX, Uribesalgo I, Coma M, Muñoz FJ (2005) The physiology and pathophysiology of nitric oxide in the brain. Prog Neurobiol 76:126–152.

Harris KM, Kater SB (1994) Dendritic spines: cellular specializations imparting both stability and flexibility to synaptic function. Ann Rev Neurosci 17:341–371.

Hui CW, Bhardwaj SK, Sharma K, Joseph AT, Bisht K, Picard K, Tremblay MÈ, Srivastava LK (2019) Microglia in the developing prefrontal cortex of rats show dynamic changes following neonatal disconnection of the ventral hippocampus. Neuropharmacology 146:264–275.

Juncal-Ruiz M, Riesco-Dávila L, Ortiz-García de la Foz V, Martínez-Garcia O, Ramírez-Bonilla M, Ocejo-Viñals JG, Leza JC, López-Hoyos M, Crespo-Facorro B (2018) Comparison of the anti-inflammatory effect of aripiprazole and risperidone in 75 drug-naive first episode psychosis individuals: a 3months randomized study. Schizophr Res 202:226–233.

Kelleher RJ 3rd, Govindarajan A, Jung HY, Kang H, Tonegawa S (2004) Translational control by MAPK signaling in long-term synaptic plasticity and memory. Cell 116:467–479.

Konopaske GT, Balu DT, Presti KT, Chan G, Benes FM, Coyle JT (2018) Dysbindin-1 contributes to prefrontal cortical dendritic arbor pathology in schizophrenia. Schizophr Res 201:270–277.

Kuroki T, Nagao N, Nakahara T (2008) Neuropharmacology of second-generation antipsychotic drugs: a validity of the serotonin–dopamine hypothesis. Prog Brain Res 172:199–212.

Lee SB, Xuan Nguyen TL, Choi JW, Lee KH, Cho SW, Liu Z, Ye K, Bae SS, Ahn JY (2008) Nuclear Akt interacts with B23/NPM and protects it from proteolytic cleavage, enhancing cell survival. Proc Natl Acad Sci U S A 105:16584–16589.

Le Pen G, Grottick AJ, Higgins GA, Martin JR, Jenck F, Moreau JL (2000) Spatial and associative learning deficits induced by neonatal excitotoxic hippocampal damage in rats: further evaluation of an animal model of schizophrenia. Behav Pharmacol 11:257–268.

Le Pen G, Kew J, Alberati D, Borroni E, Heitz MP, Moreau JL (2003) Prepulse inhibition deficits of the startle reflex in neonatal ventral hippocampal-lesioned rats: reversal by glycine and a glycine transporter inhibitor. Biol Psychiatry 54:1162–1170.

Leza JC, García-Bueno B, Bioque M, Arango C, Parellada M, Do K, O'Donnell P, Bernardo M (2015) Inflammation in schizophrenia: a question of balance. Neurosci Biobehav Rev 55:612–626.

Lipska BK, Jaskiw GE, Weinberger DR (1993) Postpubertal emergence of hyperresponsiveness to stress and to amphetamine after neonatal excitotoxic hippocampal damage: a potential animal model of schizophrenia. Neuropsychopharmacology 9:67–75.

Lipska BK, Khaing ZZ, Weickert CS, Weinberger DR (2001) BDNF mRNA expression in rat hippocampus and prefrontal cortex: effects of neonatal ventral hippocampal damage and antipsychotic drugs. Eur J Neurosci 14:135–144.

MacDowell KS, García-Bueno B, Madrigal JL, Parellada M, Arango C, Micó JA, Leza JC (2013) Risperidone normalizes increased inflammatory parameters and restores anti-inflammatory pathways in a model of neuroinflammation. Int J Neuropsychopharmacol 16:121–135.

Martinez-Cengotitabengoa M, MacDowell KS, Alberich S, Diaz FJ, Garcia-Bueno B, Rodriguez-Jimenez R, Bioque M, Berrocoso E, Parellada M, Lobo A, Saiz PA, Matute C, Bernardo M, Gonzalez-Pinto A, Leza JC; FLAMM-PEPs (2016) BDNF and NGF signalling in early phases of psychosis: relationship with inflammation and response to antipsychotics after 1 year. Schizophr Bull 42:142–151.

Martin-Hernandez D, Tendilla-Beltrán H, Madrigal JLM, García-Bueno B, Leza JC, Caso JR (2019) Chronic mild stress alters kynurenine pathways changing the glutamate neurotransmission in frontal cortex of rats. Mol Neurobiol 56:490–501.

Matsuzaki M, Honkura N, Ellis-Davies GC, Kasai H (2004) Structural basis of long-term potentiation in single dendritic spines. Nature 429:761–766.

McDannald MA, Whitt JP, Calhoon GG, Piantadosi PT, Karlsson RM, O'Donnell P, Schoenbaum G (2011) Impaired reality testing in an animal model of schizophrenia. Biol Psychiatry 70:1122–1126.

McNamara RK, Able JA, Jandacek R, Rider T, Tso P (2009) Chronic risperidone treatment preferentially increases rat erythrocyte and prefrontal cortex omega-3 fatty acid composition: evidence for augmented biosynthesis. Schizophr Res 107:150–157.

McNamara RK, Jandacek R, Rider T, Tso P (2011) Chronic risperidone normalizes elevated pro-inflammatory cytokine and C-reactive protein production in omega-3 fatty acid deficient rats. Eur J Pharmacol 652:152–156.

Middlemas DS, Lindberg RA, Hunter T (1991) TrkB, a neural receptor protein-tyrosine kinase: evidence for a full-length and two truncated receptors. Mol Cell Biol 11:143–153.

Miller BJ, Buckley P, Seabolt W, Mellor A, Kirkpatrick B (2011) Meta-analysis of cytokine alterations in schizophrenia: clinical status and antipsychotic effects. Biol Psychiatry 70:663–671.

Morales-Medina JC, Mejorada A, Romero-Curiel A, Aguilar-Alonso P, León-Chávez BA, Gamboa C, Quirion R, Flores G (2008) Neonatal administration of *N*-omega-nitro-L-arginine induces permanent decrease in NO levels and hyperresponsiveness to locomotor activity by D-amphetamine in postpubertal rats. Neuropharmacology 55:1313–1320.

Negrete-Díaz JV, Baltazar-Gaytán E, Bringas ME, Vazquez-Roque RA, Newton S, Aguilar-Alonso P, León-Chávez BA, Flores G (2010) Neonatal ventral hippocampus lesion induces increase in nitric oxide [NO] levels which is attenuated by subchronic haloperidol treatment. Synapse 64:941–947.

Nicoll RA (2017) A brief history of long-term potentiation. Neuron 93:281–290.

Noto C, Ota VK, Gouvea ES, Rizzo LB, Spindola LM, Honda PH, Cordeiro Q, Belangero SI, Bressan RA, Gadelha A, Maes M, Brietzke E (2014) Effects of risperidone on cytokine profile in drug-naive first-episode psychosis. Int J Neuropsychopharmacol 18:pyu042.

O'Donnell P (2012) Cortical disinhibition in the neonatal ventral hippocampal lesion model of schizophrenia: new vistas on possible therapeutic approaches. Pharmacol Ther 133:19–25.

Paxinos G, Watson C (1986) The rat brain atlas. San Diego: Academic.

Plum F (1972) Prospects for research on schizophrenia: 3. Neurophysiology. Neuropathological findings. Neurosci Res Program Bull 10:384–388.

Potkin SG, Turner JA, Brown GG, McCarthy G, Greve DN, Glover GH, Manoach DS, Belger A, Diaz M, Wible CG, Ford JM, Mathalon DH, Gollub R, Lauriello J, O'Leary D, van Erp TG, Toga AW, Preda A, Lim KO; FBIRN (2009) Working memory and DLPFC inefficiency in schizophrenia: the FBIRN study. Schizophr Bull 35:19–31.

Remington G, Foussias G, Fervaha G, Agid O, Takeuchi H, Lee J, Hahn M (2016) Treating negative symptoms in schizophrenia: an update. Curr Treat Options Psychiatry 3:133–150.

Romero-Pimentel AL, Vázquez-Roque RA, Camacho-Abrego I, Hoffman KL, Linares P, Flores G, Manjarrez E (2014) Histological correlates of N40 auditory evoked potentials in adult rats after neonatal ventral hippocampal lesion: animal model of schizophrenia. Schizophr Res 159:450–457.

Rueter LE, Ballard ME, Gallagher KB, Basso AM, Curzon P, Kohlhaas KL (2004) Chronic low dose risperidone and clozapine alleviate positive but not negative symptoms in the rat neonatal ventral hippocampal lesion model of schizophrenia. Psychopharmacology 176:312–319.

Ryan RT, Bhardwaj SK, Tse YC, Srivastava LK, Wong TP (2013) Opposing alterations in excitation and inhibition of layer 5 medial prefrontal cortex pyramidal neurons following neonatal ventral hippocampal lesion. Cereb Cortex 23:1198–1207.

Sams-Dodd F, Lipska BK, Weinberger DR (1997) Neonatal lesions of the rat ventral hippocampus result in hyperlocomotion and deficits in social behaviour in adulthood. Psychopharmacology 132:303–310.

Sandberg M, Patil J, D'Angelo B, Weber SG, Mallard C (2014) NRF2-regulation in brain health and disease: implication of cerebral inflammation. Neuropharmacology 79:298–306.

Sekar A, Bialas AR, de Rivera H, Davis A, Hammond TR, Kamitaki N, Tooley K, Presumey J, Baum M, Van Doren V, Genovese G, Rose SA, Handsaker RE; Schizophrenia Working Group of the Psychiatric Genomics Consortium (2016) Schizophrenia risk from complex variation of complement component 4. Nature 530:177–183.

Sellgren CM, Gracias J, Watmuff B, Biag JD, Thanos JM, Whittredge PB, Fu T, Worringer K, Brown HE, Wang J, Kaykas A, Karmacharya R, Goold CP, Sheridan SD, Perlis RH (2019) Increased synapse elimination by microglia in schizophrenia patient-derived models of synaptic pruning. Nat Neurosci 22:374–385.

Sheng M, Hoogenraad CC (2007) The postsynaptic architecture of excitatory synapses: a more quantitative view. Ann Rev Biochem 76:823–847.

Sholl A, Uttley AM (1953) Pattern discrimination and the visual cortex. Nature 171:387–388.

Sierra A, Camacho-Abrego I, Escamilla C, Negrete-Diaz JV, Rodriguez-Sosa L, Flores G (2009) Economical body platform for neonatal rats stereotaxic surgery [in Spanish]. Rev Neurol 48:141–146.

Tang S, Yasuda R (2017) Imaging ERK and PKA activation in single dendritic spines during structural plasticity. Neuron 93:1315–1324.e3.

Tendilla-Beltrán H, Antonio Vazquez-Roque R, Judith Vázquez-Hernández A, Garcés-Ramírez L, Flores G (2019) Exploring the dendritic spine pathology in a schizophrenia-related neurodevelopmental animal model. Neuroscience 396:36 – 45.

Tseng KY, Chambers RA, Lipska BK (2009) The neonatal ventral hippocampal lesion as a heuristic neurodevelopmental model of schizophrenia. Behav Brain Res 204:295–305.

Vanderschuren LJ, Niesink RJ, Van Ree JM (1997) The neurobiology of social play behavior in rats. Neurosci Biobehav Rev 21:309 –326.

Vázquez-Roque RA, Ramos B, Tecuatl C, Juárez I, Adame A, de la Cruz F, Zamudio S, Mena R, Rockenstein E, Masliah E, Flores G (2012) Chronic administration of the neurotrophic agent cerebrolysin ameliorates the behavioral and morphological changes induced by neonatal ventral hippocampus lesion in a rat model of schizophrenia. J Neurosci Res 90:288 –306.

Vázquez-Roque RA, Ubhi K, Masliah E, Flores G (2014) Chronic cerebrolysin administration attenuates neuronal abnormalities in the basolateral amygdala induced by neonatal ventral hippocampus lesion in the rat. Synapse 68:31–38.

Weinberger DR (1987) Implications of normal brain development for the pathogenesis of schizophrenia. Arch Gen Psychiatry 44:660 – 669.

Weinhard L, di Bartolomei G, Bolasco G, Machado P, Schieber NL, Neniskyte U, Exiga M, Vadisiute A, Raggioli A, Schertel A, Schwab Y, Gross CT (2018) Microglia remodel synapses by presynaptic trogocytosis and spine head filopodia induction. Nat Commun 9:1228.

Wible CG, Anderson J, Shenton ME, Kricun A, Hirayasu Y, Tanaka S, Levitt JJ, O'Donnell BF, Kikinis R, Jolesz FA, McCarley RW (2001) Prefrontal cortex, negative symptoms, and schizophrenia: an MRI study. Psychiatry Res 108:65–78.

Wong J, Rothmond DA, Webster MJ, Weickert CS (2013) Increases in two truncated TrkB isoforms in the prefrontal cortex of people with schizophrenia. Schizophr Bull 39:130 –140.

Ying SW, Futter M, Rosenblum K, Webber MJ, Hunt SP, Bliss TV, Bramham CR (2002) Brain-derived neurotrophic factor induces long-term potentiation in intact adult hippocampus: requirement for ERK activation coupled to CREB and upregulation of *Arc* synthesis. J Neurosci 22:1532–1540.

Yuan P, Zhou R, Wang Y, Li X, Li J, Chen G, Guitart X, Manji HK (2010) Altered levels of extracellular signal-regulated kinase signaling proteins in postmortem frontal cortex of individuals with mood disorders and schizophrenia. J Affect Disord 124:164 –169.